Predicting the Distribution of Russian Olive Stands in Eastern Montana Valley Bottoms Using NAIP Imagery

Prepared for:

The U.S. Environmental Protection Agency

Agreement Number:

95815401

Prepared by:

Claudine Tobalske and Linda Vance

October 2017

P.O. Box 201800 ● 1515 East Sixth Avenue ● Helena, MT 59620-1800 ● 406-444-5354

Table of Contents

List of Tables

List of Figures

EXECUTIVE SUMMARY

Russian olive (*Elaeagnus angustifolia*), a Eurasian native, has been cultivated in North America since colonial times. Its presence has been noted in Montana since 1959, and by the mid-1980s, Russian olive had begun to naturalize in the state. However, a global view of its distribution in eastern Montana is currently lacking. We investigated the utility of remote sensing technology, specifically NAIP imagery, for generating a clearer picture of Russian olive in eastern Montana.

Our study addressed the following questions:

I. Can NAIP be used to generate a current distribution map of Russian olive along eastern Montana rivers?
II. Can a predictive model of Russian olive infestation along eastern Montana rivers be developed and used to identify areas threatened by colonization?
III. Can NAIP be used to follow the evolution of the distribution of Russian olive along eastern Montana rivers? Evolution includes both increase (invasion of new sites, spatial expansion of established patches) and decrease (removal through natural flooding or through active management).

We first segmented NAIP 2013 imagery using eCognition and developed a RandomForest model in Weka to generate a land cover map of valley bottoms for ten eastern Montana rivers, Russian olive being one of the land cover classes mapped. Classification accuracy for Russian olive was 75% or higher, making it possible to compare infestation among rivers.

Next, we entered our mapped Russian olive data along with 16 other variables into Maxent to generate a predictive model of potential Russian olive infestation. Because this is a probabilistic model of future infestation, it is not possible to assess its accuracy, especially at the scale of entire valley bottoms. However, it can be used to direct attention to specific areas that could be more at risk of infestation than others.

Finally, to assess whether NAIP can be used to follow changes in Russian olive coverage, we focused on two rivers, the Marias (which is regulated) and the Musselshell (unregulated and subject to intense flooding episodes). In both cases we found that NAIP imagery is accurate enough, even if flown in late season, to detect areas where Russian olive has been removed (whether naturally through flooding or through active management actions), as well as areas where it has expanded its colonization. To reach a sufficient degree of accuracy at the patch level, however, it was necessary to manually edit the classification output onscreen. Nevertheless, the segmentation approach was faster than straight onscreen digitizing would be, and because of the scale of imagery (1m pixels), a better solution than a pixel-based classification.

Nationally, NAIP imagery is contracted each year based upon available funding; originally acquired on a 5-year cycle, it was updated to a 3-year cycle in 2008. For Montana it was most recently flown in 2015/16, so the next cycle will probably occur around 2018/19. Until then, fine-scale mapping like that conducted for the Marias and Musselshell could be repeated for other Montana rivers.

INTRODUCTION

Russian olive (*Elaeagnus angustifolia*), a small tree native to southern Europe and western Asia, was introduced into North America during colonial times (Elias 1980). Originally planted for windbreaks, ornamental appeal, wildlife habitat, or erosion control, it has escaped cultivation and is naturalizing rapidly, especially in riparian zones (Christiansen 1963). Booth and Wright noted its cultivation in Montana in 1959, but did not report instances of escape; by the mid-1980s, however, it had begun naturalizing, chiefly along the Musselshell River and around Bowdoin National Wildlife Refuge, with some scattered areas in northern and eastern parts of the state (Olson and Knopf 1986). Introduced onto one site on the Milk River floodplain in 1950, Russian olive was found 160km downriver 50 years later (Pearce and Smith 2001). Important concentrations of Russian olive trees were also observed along the Sun, Musselshell, Bighorn, Yellowstone and Missouri Rivers, but only two stands were seen on the Tongue and Powder Rivers and only two isolated trees were noted on the Little Missouri River (Pearce and Smith 2001). Lesica and Miles (2001, 2003) studied Russian olive distribution along the Marias and the lower Yellowstone Rivers and speculated that Russian olive will establish with increasing frequency in riparian forests in eastern Montana, where it will replace the native cottonwood forests unless regular flooding reinitiates primary succession of native trees They noted, however, that because of its long maturation time and low recruitment rate, Russian olive invasion in Montana will not proceed as fast as other exotic species.

While offering valuable insights into Russian olive establishment and spreading, these studies do not offer a global view of the current distribution of Russian olive in eastern Montana. Furthermore, traditional methods of vegetation mapping such as field surveys are time consuming, expensive, and therefore are usually geographically limited. However, remote sensing technology offers an economical means to map vegetation cover, especially over large areas. The challenge of remote sensing lies in acquisition of base imagery for classification. Landsat imagery is now available free of charge for the entire United States, with a two-week periodicity from 1984 to the present, but its resolution (30m pixels, i.e. 0.09 ha, or 0.22 acres) is too coarse to map anything but the largest Russian olive stands. In 2003, however, the United States Department of Agriculture started acquiring 1m pixel aerial imagery during the agricultural growing season in the continental U.S. The National Agriculture Imagery Program (NAIP) was first flown over Montana in 2005 as a natural color three-band product (Red, Green and Blue), with a near infrared band collected separately. Since then, a four-band product has been flown 4 times, in 2009, 2011, 2013, and 2015. For classification purposes, vegetation types must produce distinct spectral or visual signatures so that the remotely sensed images can be differentiated (Xie et al. 2008). Russian olive leaves are covered in distinctive silvery-gray scales (Great Plain Flora Association 1986) which, combined with the roundish shape of mature trees, makes them easily identifiable by the human eye on NAIP imagery, at least earlier in the growing season.

The ease with which Russian olive can be differentiated from other species in high-resolution imagery now makes it possible to answer broad questions about its distribution and spread in Montana. Furthermore, the availability of current ancillary data layers (e.g., roads, structures,

wetlands, etc.) allows the testing of hypotheses about the ways in which new stands are established, and more particularly, about the best ways to prevent further spreading. Therefore, this project was designed to answer three questions:

1. Can NAIP be used to generate a current distribution map of Russian olive along eastern Montana rivers?
2. Can we build a predictive model of Russian olive infestation along eastern Montana rivers that could identify areas threatened by colonization, or areas where mechanical eradication would prove the most beneficial?
3. Can NAIP be used to track invasion of new sites and spatial expansion of established patches, as well as recording any decrease in stands resulting from natural flooding or active management?

Each of these questions is treated separately in the following sections.

I. MAPPING THE DISTRIBUTION OF RUSSIAN OLIVE STANDS IN EASTERN MONTANA VALLEY BOTTOMS

Our intent was to generate a map of current Russian olive distribution along major eastern Montana rivers, with a goal of 85% user's accuracy.

Project area

The project focused on ten large rivers in eastern Montana: the Bighorn, Clark Fork of the Yellowstone, Judith, Marias, Milk, Missouri, Musselshell, Powder, Tongue, and Yellowstone rivers (Figure 1). Previous vegetation mapping (using NAIP 2009) showed that they are all currently suffering from various degrees of Russian olive infestation (Vance and Tobalske, unpublished data). Four other rivers (Big Muddy, Little Missouri, Little Powder, and Poplar) were examined onscreen using NAIP imagery but Russian olive was not detected. The Tongue River was only mapped for about 21 miles from its confluence with the Yellowstone (as the crow flies), and mapping could even have stopped at 15 miles as no Russian olive was detected upstream during NAIP inspection or bank surveys (Vance, pers. obs.). We also did not map the Missouri River from Holter Dam to Coal Banks Coulee. While individual Russian olive trees occur along this stretch, they are too isolated for automated classification.

Figure 1. Location of the ten eastern Montana valley bottoms mapped for Russian olive.

Methods

Valley bottom delineation

First, valley bottoms were delineated by hand using NAIP imagery and 1m and 5m contour lines derived from a 10m DEM (Figure 2).

Image preparation

The 2015 NAIP was incomplete for some areas of Montana due to cloud cover, wildfire smoke, and snow cover; a supplement was flown in 2016. For the purposes of this project, a composite image constructed from two separate years would be sufficient. However, in both 2015 and 2016, flight and image acquisition conditions were poor during summer months, and consequently most flights were conducted in August, September and October (Figure 3, Table 1). By contrast, almost all the 2013 NAIP tiles overlapping eastern Montana rivers were collected in June or July (Figure 4, Table 1).

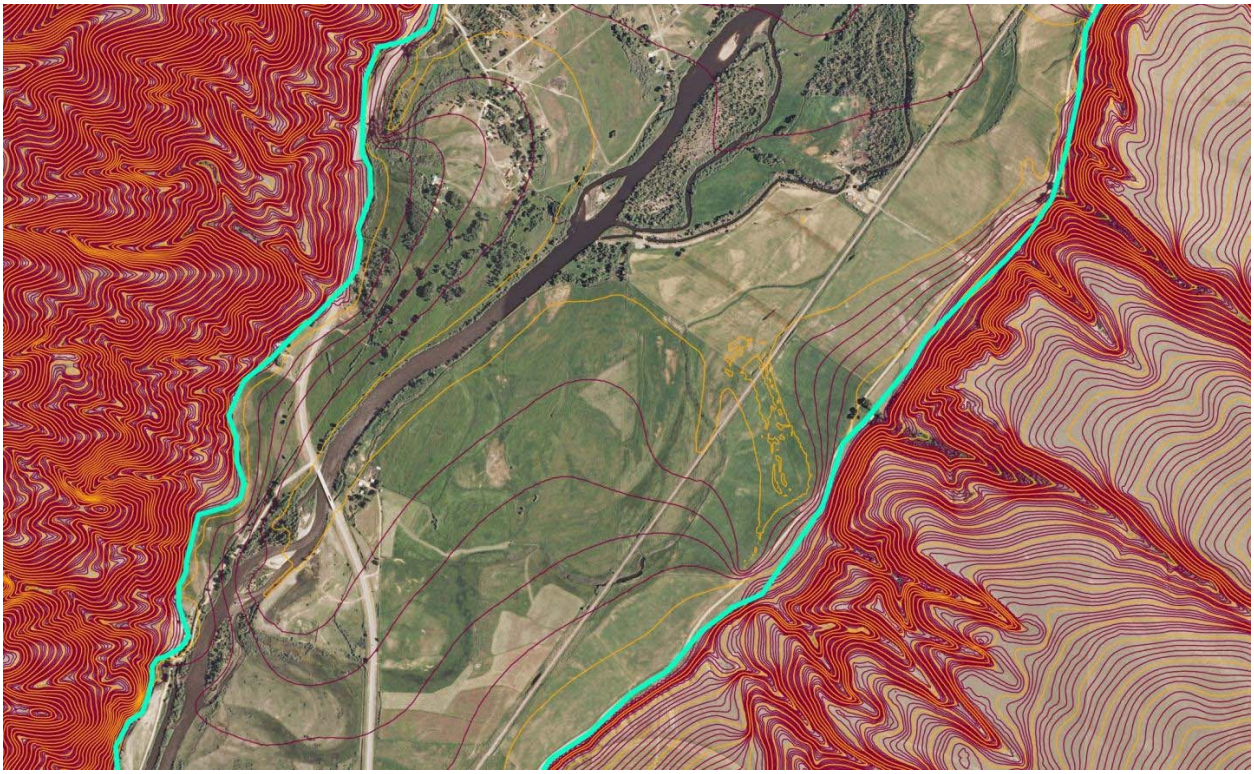

Figure 2. Valley bottom delineation based on 1m and 5m contour lines and NAIP imagery.

*Table 1. Percent of ten eastern Montana valley bottoms flown each month for NAIP imagery 2013 (**black**) and 2015 (**red**).*

	June		July		August		September		October
Big Horn	100	99.82						0.18	
Clark Fork	100			74.30		25.70			
Judith	100			88.31		11.69			
Marias			100					84.92	15.08
Milk			100					88.07	11.93
Missouri	6.2		93.8	8.75		3.02		66.06	22.16
Musselshell	39.88	41.39	60.12	20.99		15.03		22.59	
Powder	100			36.51				53.91	
Tongue	100							41.47	58.26
Yellowstone	36.78	4.88	58.28	19.26	2.5	19.80	2.44	38.29	17.77

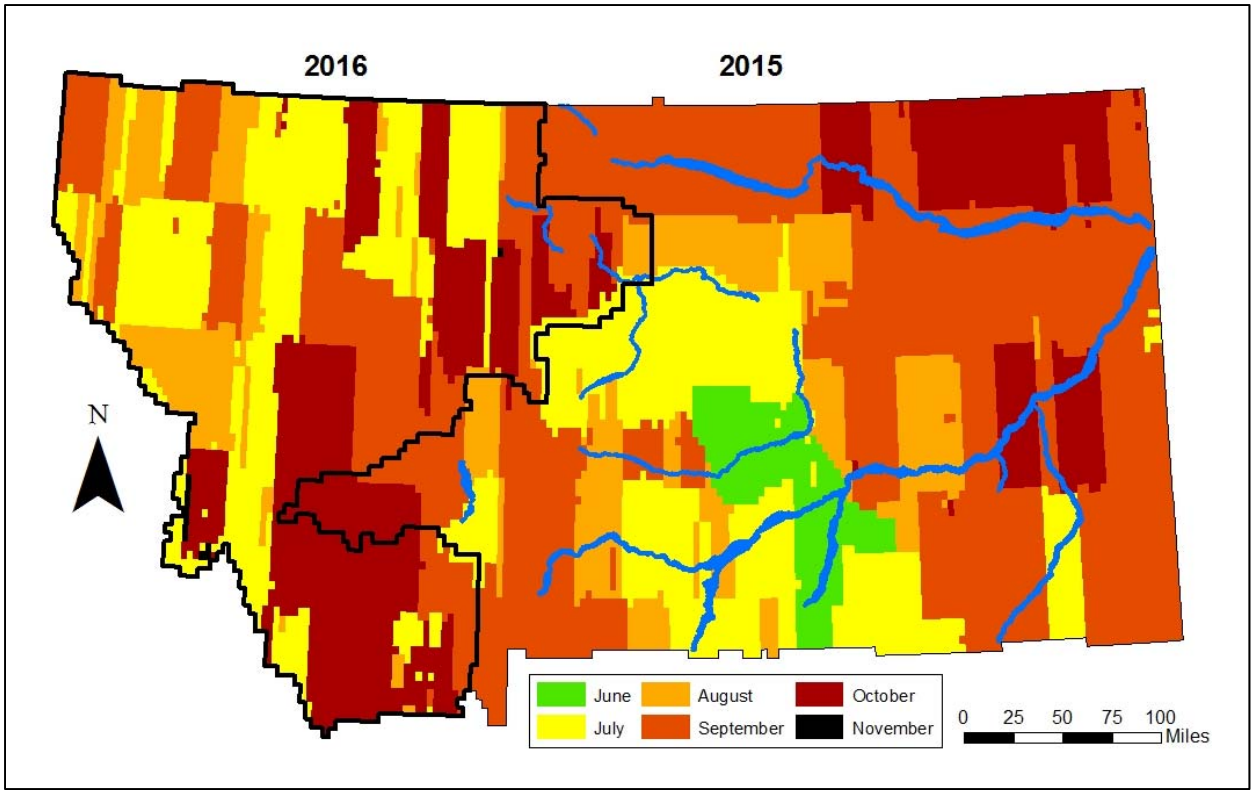

Figure 3. Years and months during which the 2015 NAIP imagery was collected.

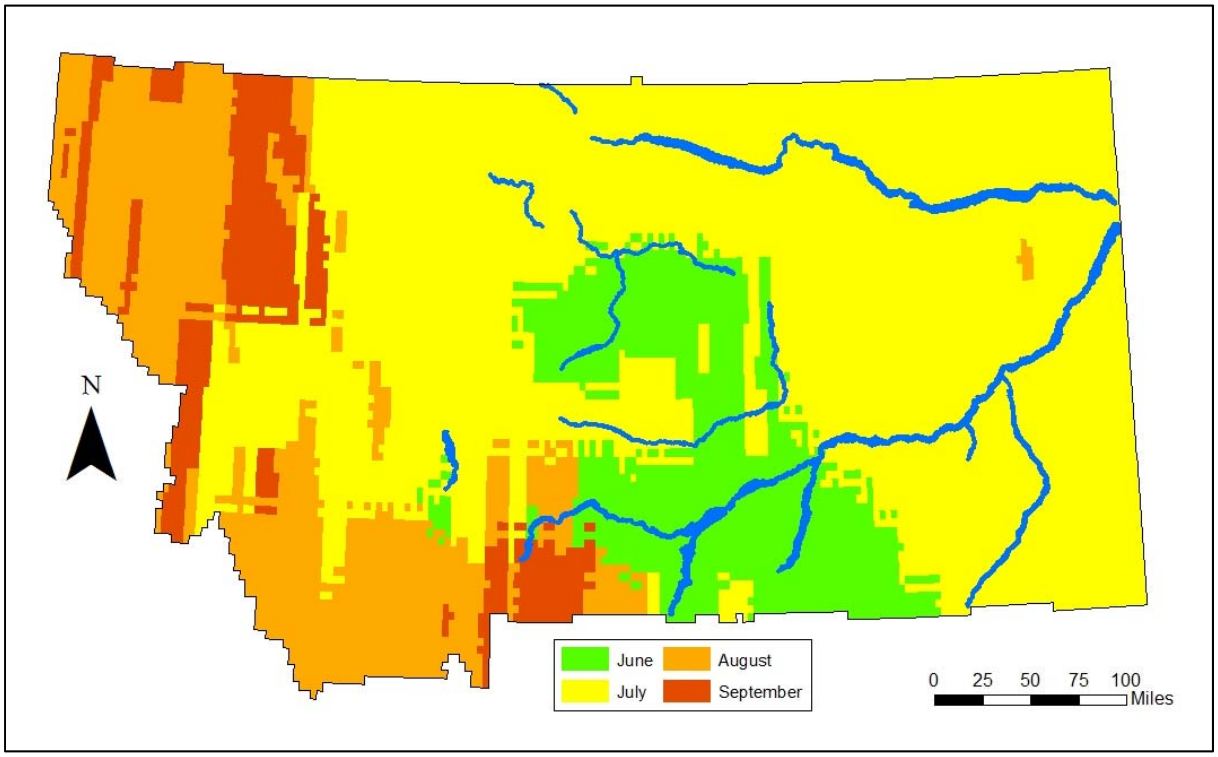

Figure 4. Months during which the 2013 NAIP imagery was collected.

This presented a problem for mapping Russian olive distribution. Not only does the leaves' distinctive silvery color tend to fade in late summer and fall, but the leaves of other species of deciduous trees and shrubs turn from green to yellow, making differentiation difficult, especially in areas where Russian olive is not the only shrub or small tree (Figure 5).

Figure 5. NAIP imagery flown on July 19th, 2013 (left) and September 20th, 2015 (right) showing the loss of contrast between Russian olive and surrounding vegetation as the growing season progresses.

Because of this issue, we decided to base our mapping on 2013 NAIP imagery. Russian olive is a slow-growing tree that takes about 10 years to become reproductively mature in north-central Montana (Lesica and Miles 2003), so not using the most recent imagery source should not have great consequences on a general overview of the species' distribution. The four-band, 2013 raw NAIP imagery was extracted for each valley bottom and a pseudo-NDVI was computed in ArcGIS Raster Calculator using the following formula: *(Near Infra-Red band 4 – Red band 1)/(Near Infra-Red band 4 + Red band 1).*

Segmentation

The traditional approach to image classification is pixel-based, either supervised or unsupervised, and relies solely on spectral characteristics of individual pixels. This greatly limits the potential for identification of spatially contiguous areas, often resulting in "salt and pepper" classification, with many small regions or even single pixels classified as events. By contrast, object-based image analysis classifies objects instead of single pixels, making it possible to use textural and contextual information in addition to spectral information. When comparing these two approaches using images at various scales, Gao and Mas (2008) concluded that the advantages of object-based image analysis over pixel-based classification are presented by higher resolution images (i.e., smaller pixel size). First grouping pixels with similar spectral information into objects that were then analyzed resulted in higher classification accuracy for images with high spatial resolution; on the other hand, images with medium to low spatial resolution exhibited lower spectral variability and were easily handled by pixel-based methods. With its 1m pixels, NAIP imagery has high spatial resolution, making it a prime candidate for object-oriented analysis.

The first step of object-oriented classification is segmentation, the process of grouping pixels into meaningful polygons ("objects") that are homogeneous with regards to one or more characteristics, typically spectral information. In this study, we used the four NAIP band values; the pseudo-NDVI was used for classification only. Segmentation was conducted in eCognition 9.0 and followed a "bottom up" approach, wherein small polygons were progressively grouped into larger ones. Segmentation scale, an abstract value that determines the maximum possible change of heterogeneity caused by fusing several objects, was determined through trial-and-error. Too small a scale resulted in homogeneous patches of vegetation being artificially split into numerous polygons, causing problems during classification. On the other hand, too large a scale resulted in heterogeneous polygons. The best compromise was obtained for a scale of 100. Particularly long rivers had to be divided into sections prior to segmentation to avoid size limitations (3 sections each for the Milk and Missouri rivers, 8 sections for the Yellowstone River). The number of polygons was also reduced by "masking out" agricultural areas prior to segmentation, using the most recent Department of Revenue FLU GIS layer. In addition to scale, the segmentation algorithm uses two parameters, Shape and Compactness, that are used to influence the shape of polygons. Both their values range from 0 to 1; a low Shape value (e.g., 0.1) places a high emphasis on color which is normally the most important for creating meaningful objects (Definiens AG, 2009). Higher Compactness weightings (e.g., 0.9) result in more compact object boundaries. Again using trial-and-error, we settled on a Shape value of 0.3 and kept the default value of 0.5 for Compactness.

Training points

After segmenting a valley bottom, resulting polygon outlines were displayed on top of the NAIP imagery and training points were manually digitized within polygons representative of a given class (Figure 6). We used the following 7 classes:

- *Water*.
- *Sand Bars*: unvegetated, sandy or gravelly islands or river shores.
- *Shrub-Scrub*: all riparian shrubby patches; could also include polygons with rare trees scattered in a shrubby understory.
- *Forested:* all forested patches, including closed forest, relatively open forest, or in the case of a predominantly grassy area, single trees.
- *Russian Olive*: patches of Russian olive with varying degrees of density; could be pure stands, mixed shrubland patches dominated by Russian olive, or single Russian olive trees.
- *Riparian Emergent*: patches of grassland in a riparian setting; also included vegetated sand bars (unless classified as shrubland or forested). Human-caused greenness (such as lawns, golf courses, and stadiums) was also classified as riparian emergent.
- *Upland Emergent*: non-riparian grassland areas. By default, all barren surfaces not classified as sand bars also fell into this category (e.g., paved surfaces, roofs, rocky areas, sand pits).

Number of points per class varied by valley bottom, with more points typically digitized for larger ones. We made a deliberate effort to digitize enough points to cover as much of the spectral variability of each class as possible. If a class was poorly represented within a particular valley bottom (i.e., fewer than 25 segments), it did not enter the classification process; instead, polygons corresponding to the rare class(es) were manually recoded during post-modeling.

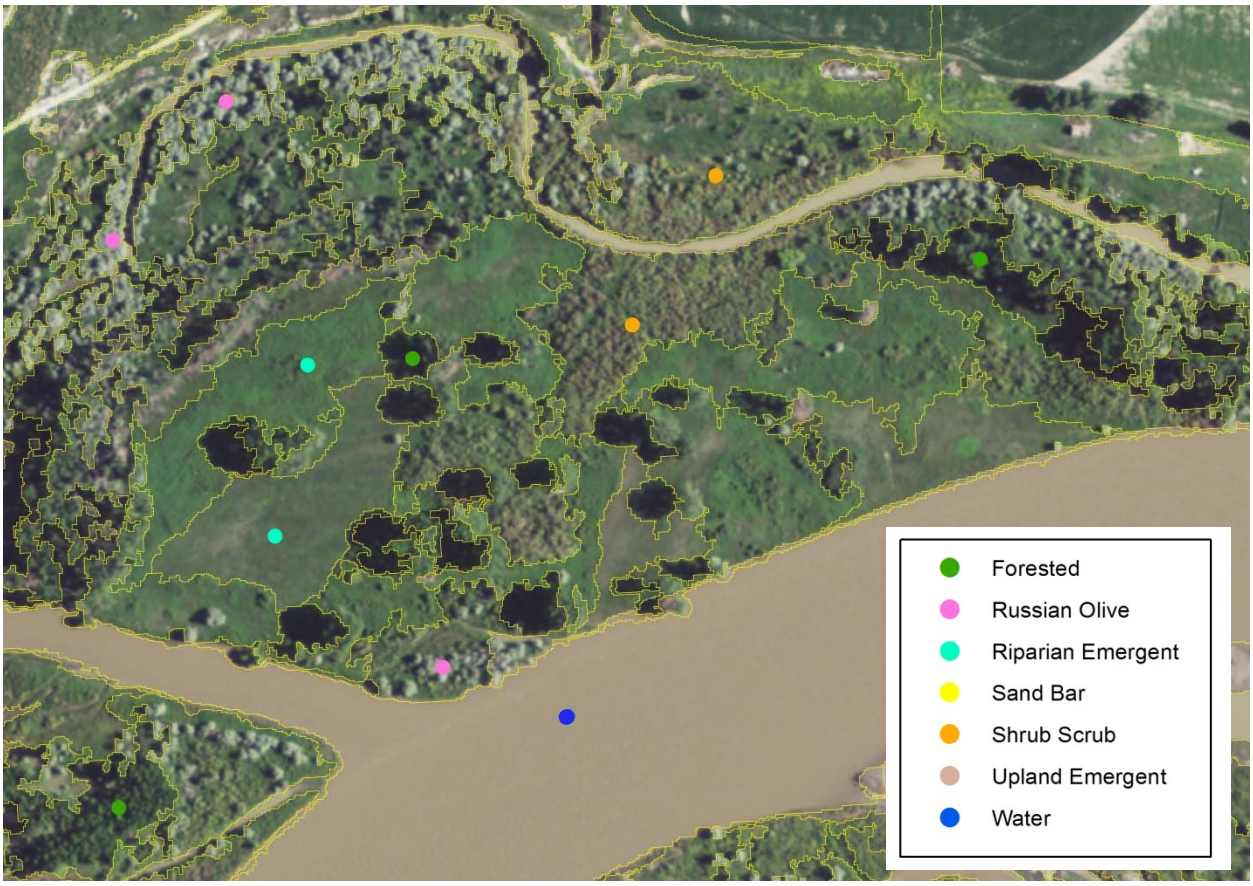

Figure 6. An example of training points digitized onscreen using NAIP 2013.

Classification

Thirty-five attributes were extracted for each object: layer values (*mean* and *standard deviation* of each NAIP band as well as *NDVI*, plus *brightness* and *maximum difference*); geometry (*area, border length, length, number of pixels, volume, width, length/width*); shape (*asymmetry, compactness, density, elliptic fit, main direction, radius of largest enclosed ellipse, radius of smallest enclosing ellipse, rectangular fit, roundness, shape index, border index*); and texture after Haralick (*GLCM contrast, GLCM entropy, GLCM mean, GLCM correlation, GLCM homogeneity*). These attributes were extracted for each training point and imported into Weka, an open-source data mining software from the University of Waikato, NZ. Classification was done using the RandomForest algorithm with number of trees set at 200 and a 10-fold internal cross-validation. A Java command extrapolated the result of the classification to all the segments in the valley bottom and the resulting classification was displayed in ArcGIS.

Post-modeling

For all valley bottoms the most common confusions were: Water and Forested or Upland Emergent (shadows, roofs); Sand Bars and Upland Emergent; Shrub-Scrub and Forested; Russian Olive and Forested or Riparian Emergent. Depending on the size and prominence of sand bars in a given valley bottom, a distance was selected (from 10m to 100m) and all segments classified as "Sand Bars" but further away from water by this distance were reclassified as "Upland Emergent". All other misclassifications were corrected manually, by doing a "once over" of the valley bottom for each class, with the NAIP imagery in the backdrop. Although tedious, this approach was more satisfactory than any automated approach, and guaranteed the best results. Particular attention was given to correctly mapping Russian olive patches. Agricultural polygons from the most recent Montana Department of Revenue Final Land Units (DOR-FLU) layer were merged with the classification output. Roads and railroads were extracted from the most recent Montana Spatial Data Infrastructure transportation framework database (02/2015); roads were buffered based on their width, 10m per lane up to 40m maximum and railroads were buffered by 20m. Both layers were "burned in" to the final land cover layer. Finally, structure points from the most recent Montana Spatial Data Infrastructure structures framework database (04/2015) were used to reclassify underlying "Upland Emergent" polygons to "Developed".

Results and accuracy assessment

We aimed to reach a user's accuracy of at least 85% for Russian olive. User's accuracy is a measure of the reliability of an output map generated from a classification scheme; or, in practical terms, the likelihood of a "user" going to a site and finding a correctly classified polygon. Confusion tables, with users' and producers' accuracies for each class, as well as overall accuracy and Cohen's Kappa, were obtained for each river (or river section) prior to post-modeling. These accuracy measures were generated by the software using a 10-fold cross-validation procedure: training data are randomly partitioned into 10 sets; a model is developed using 9 sets and applied to the 10^{th} set; this is repeated 10 times and the validation results are averaged.

Ten out of 21 sections did not have enough Russian olive polygons to warrant modeling. For the remaining 11, Russian olive user's accuracies ranged from 74.29% (Yellowstone, Center 2) to 100% (Milk, West; Table 2). The Musselshell River and the Yellowstone River, West 3, were the other two sections with a user's accuracy lower than 85% (Table 2). Overall classification accuracies (i.e., for all classes together) ranged from 80.89% (Musselshell) to 93.3% (Yellowstone, East 3), with only one other section below 85% (Yellowstone, Center 2). Cohen's Kappa, a measure of improvement over chance classification, was greater than 0.8 for all rivers/sections but the Musselshell (0.7726).

We performed independent validation after post-modeling. Points were digitized onscreen as for training, after masking out those polygons used for model development; a single set was digitized for the Milk and Yellowstone rivers but not for the Missouri. Twenty points per class were then randomly selected using the ***r.sample*** command of the Geospatial Modelling Environment software (40 points for the longer Yellowstone River) and overlaid with the modeling results. Overall classification accuracies ranged from 93.6% (Judith) to 99.07% (Clark Fork of the Yellowstone; Table 2). No class had an accuracy lower than 85% (17/20 polygons correctly classified), and

accuracy for Russian olive was 100% for all rivers except the Marias (19/20 = 95%, one confusion with Forested).

Table 2. Classification accuracy (overall and Russian olive user's accuracy) and Cohen's Kappa prior to post-modeling corrections, and overall accuracy following post-modeling corrections, for 20 river sections in eastern Montana. "n/a" indicates a river or section without enough Russian olive patches to warranty classification.

	Internal Validation			Independent Validation
	Russian Olive User's Accuracy	Overall Accuracy	Cohen's Kappa	Overall Accuracy
Bighorn	85.11	86.14	0.8334	97.14
Clark Fork Yellowstone	86.92	87.10	0.8303	99.07
Judith	n/a	89.33	0.8719	93.60
Marias	87.50	87.50	0.8100	96.70
Milk Center	89.09	86.94	0.8429	
Milk East	n/a	86.32	0.8194	94.29
Milk West	100.00	88.89	0.8609	
Missouri East	n/a	89.78	0.8762	94.66
Missouri South	n/a	89.08	0.8660	97.74
Missouri West	n/a	88.28	0.8561	96.48
Musselshell	76.00	80.89	0.7726	95.45
Powder	92.00	92.04	0.9021	97.56
Tongue	n/a	90.43	0.8744	95.28
Yellowstone Center 1	88.24	88.09	0.8574	
Yellowstone Center 2	74.29	84.22	0.8071	
Yellowstone East 1	n/a	87.50	0.8365	
Yellowstone East 2	n/a	89.15	0.8674	
Yellowstone East 3	n/a	93.30	0.9151	97.5
Yellowstone West 1	n/a	86.68	0.8392	
Yellowstone West 2	91.67	87.53	0.8488	
Yellowstone West 3	76.09	86.39	0.8305	

In terms of abundance and distribution, the Bighorn River appears to be the most affected by Russian olive, with over 3% of its valley bottom covered by Russian olive (8% of polygons, total area = 2,607 acres; Table 3). The Musselshell, Clark Fork of the Yellowstone, Marias, Powder and Yellowstone rivers have over 1% of their flood plain covered by Russian olive. The Milk River has less than 1%, but it has the third largest acreage of infestation (2,038 acres). The patchiness of Russian olive infestation is visible in Figure 7. Overall, 17,694 acres are infested by Russian olive.

Table 3. Spatial characteristics of Russian olive polygons in large river valley bottoms in eastern Montana. Sections of the Missouri River were not merged as they correspond to real geographic separations (see Figure 1). Area measures are given in acres.

	N Polygons		% Polygons	% Valley Bottom	Sum Area	Mean Area	SD Area	Max Area
	Russian Olive	*Total*						
Bighorn	3,448	42,685	8.08	3.08	2,607	0.76	0.67	7.17
CF Yellowstone	1,495	38,557	3.88	2.12	1,568	1.05	0.93	10.92
Judith	36	17,017	0.21	0.12	33	0.92	1.54	8.64
Marias	175	10,911	1.60	1.48	209	1.19	1.1	6.64
Milk	2,044	12,305	1.66	0.77	2,038	1	0.95	12.49
Missouri East	174	94,972	0.18	0.08	164	0.95	0.96	6.33
Missouri South	112	17,009	0.66	0.51	150	1.34	1.14	5.18
Missouri West	31	18,318	0.17	0.07	24	0.77	0.8	3.69
Musselshell	1,229	69,914	1.76	2.39	1,790	1.46	1.05	10.01
Powder	955	78,949	1.21	1.37	1,463	1.53	1.19	8.79
Tongue	35	6,483	0.54	0.48	46	1.3	1.27	5.05
Yellowstone	7,177	365,775	1.96	1.33	7,602	1.06	0.95	9.13

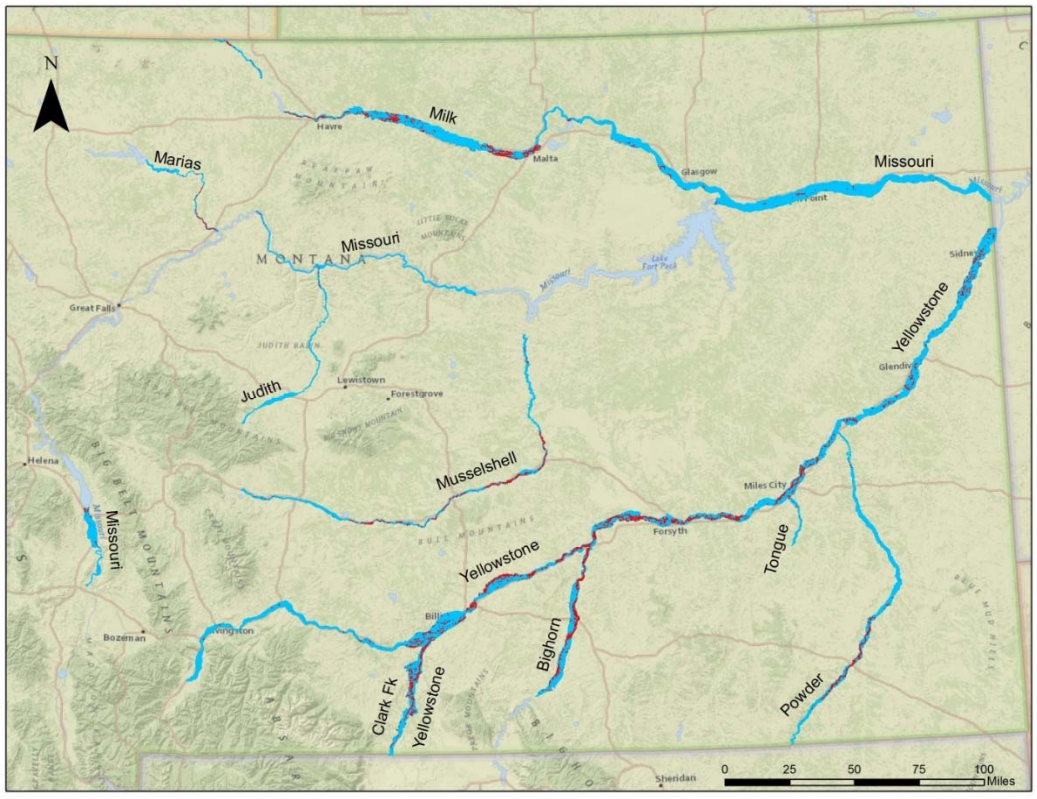

Figure 7. Distribution of Russian olive (red) in valley bottoms (light blue) of 10 large rivers in eastern Montana.

II. PREDICTIVE MODELING OF RUSSIAN OLIVE STANDS IN EASTERN MONTANA VALLEY BOTTOMS

Russian olive eradication is ongoing throughout the project area. One of the questions posed by land managers is whether or not removing Russian olive in an upstream area with heavy infestations will reduce its spread downstream. Our goal here was to determine if we could build a Maxent probabilistic predictive model for presence and absence, using a random sample of Russian olive stands and a set of topographic, climatic, edaphic, and distance variables.

Literature review

We began by reviewing previous attempts to model Russian olive distribution. Peterson et al. (2003) used values from 15 variables at a 1km-cell resolution obtained from Europe and western Asia to generate Genetic Algorithm for Ruleset Production (GARP) distribution models of four alien plant species, including Russian olive, in North America. Jarnevitch and Reynolds (2011), also working with 1km pixels, developed a habitat suitability map for Russian olive in western North America. They used 37 variables and the Maximum Entropy (Maxent) algorithm and found distance to water to be the most important predictor, along with several climate variables (mean temperature of the wettest quarter of the year, precipitation seasonality, and mean temperature of the warmest quarter of the year). In western Canada, Collette (2014) also used Maxent and 12 variables at a 1km pixel scale; mean temperature of the coldest quarter, topsoil pH, elevation, salinity, and length of regulated water per grid cell were the highest predictors. Liu et al. (2014) worked at an even coarser scale (30 km pixels), using only climate data to model Russian olive distribution for the entire United States. We could only find two studies that modeled Russian olive distribution at a finer scale. Buddhika et al. (2013) used variables at a 30m pixel resolution and Classification and Regression Tree (CART) algorithm to estimate habitat suitability for Russian olive near Bismark, ND. They found Russian olive abundance to be closely associated with silt loams and silty clay soil types. In a context closely resembling that of our own study, Hoffman et al. (2008) extracted variables within a one-mile-wide buffer along the North Platte River, NE, at the 30m-pixel size and built a predictive model in Maxent; they found elevation, distance to river and percent clay to be the best predictors.

Methods and results

Algorithm selection

Habitat models have been used extensively and effectively for predicting both general land cover and individual plant species distributions. Whereas deductive models rely on qualitative data or expert knowledge to derive rules for predicting suitability for occupancy, inductive models use statistical or machine-learning methods to identify relationships between known occurrence locations and environmental characteristics and model these relationships to allow prediction of the species' distribution across the study area (Franklin and Miller 2009). The selection of an appropriate statistical method is influenced by the type of occurrence data. Methods that require

both presence and absence data are a problem when modeling invasive plants, since sites where the species does not occur may not be environmentally unsuitable, but could be suitable sites not yet colonized (Woodbury and Weinstein 2010). This explains the popularity of Maxent, a presence-only algorithm, for invasive species distribution modeling (as opposed to RandomForest, another popular algorithm which requires absence data).

Maxent (Phillips et al. 2004) is derived from statistical mechanics and estimates the most uniform probability distribution, representing maximum entropy, for habitat suitability in a defined area, given a set of known environmental constraints (Buechling and Tobalske 2011). The software, which is freely available, was obtained online for this project from (https://www.cs.princeton.edu/~schapire/maxent/).

Predictive variables

We selected 16 environmental variables based on their suspected influence on Russian olive distribution (based on literature review) but limited by data availability. Although elevation was shown to be a strong predictor in other studies (see above), we did not include it because the model was already restricted to valley bottoms, and because of a general east-west and north-south gradient within the project area (Figure 8).

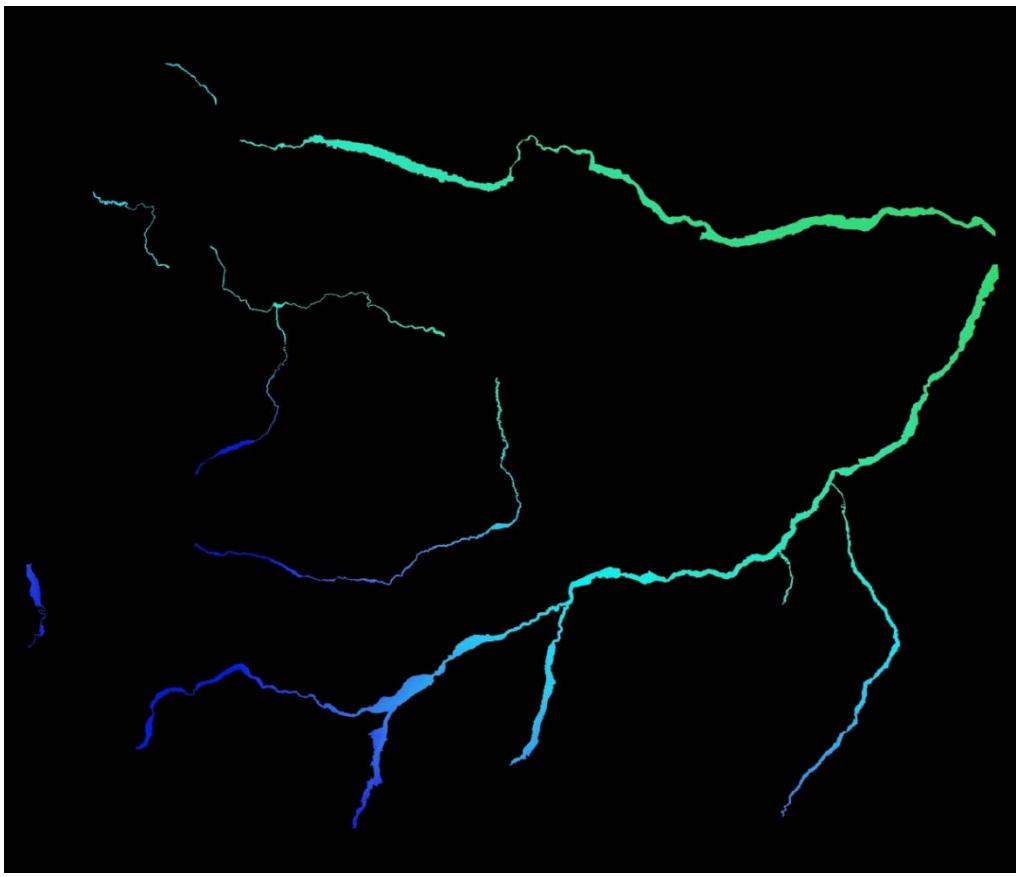

Figure 8. East-west and north-south elevation gradient across the study area, with lowest elevations in green and highest in blue.

Topographic variables included *percent slope* (derived from the USGS NED 30m DEM), *categorical aspect* (9 classes = 8, 45-degree classes plus Flat), and *valley width*. Valley width was obtained by manually dividing the valley bottoms into sections of relatively uniform width, getting the average width of each section, and assigning this value to all pixels within the section.

Russian olive prefers habitats that are moist in nature but can tolerate a wide range of soil and moisture conditions (Hoffman et al. 2008); it seems tolerant of salinity but does not tolerate long-term flooding (Pick 2013). Based on edaphic variables used in other studies, we used the USGS Soil DataViewer extension in ArcGIS and Soils Survey Geographic (SSURGO) data to generate predictive layers of *percent clay*, *percent sand*, *percent silt*, *texture* (categorical), *pH*, *electric conductivity* (as a proxy for salinity) and *flooding frequency* (categorical).

Climate variables appear to play an important role in broad-scale Russian olive distribution models; however, Montana climate data use 800m pixels and do not show enough variability at the valley bottom scale to be meaningful. The only climate variable we included was the Relative Effective Annual Precipitation (*REAP*) derived from 1km DAYMET but resampled to 30m.

Finally, we used the ArcGIS Euclidean distance command to generate grids of: 1) *distance to roads* (using all roads from the most recent MSDI Transportation Framework geodatabase, 02/06/2015), 2) *distance to canal/ditch* (from the National Hydrology Dataset High Resolution), and 3) *distance to water*, *irrigated agriculture*, and *forested* (all 3 based on the final segmentation map). Maximum distance was set at 10km.

Pixel size for all predictive layers was set at 30m, whether originally so (slope, aspect, REAP), set during creation (distance variables), or converted from vector data (edaphic variables).

Presence data

A total of 16,910 Russian olive polygons were mapped throughout the study area. Of these, 16,890 had data for all predictive variables (the remaining 20 were along the easternmost part of the study area and were missing values for REAP and SSURGO layers). 6,896 corresponded to patches larger than 1 acre, and of these, 5,962 were no closer than 90m. We randomly selected 75% (4,469) for model training and set aside 25% (1,493) for model evaluation.

Variable examination

Values for continuous variables were extracted at the centroids of all Russian olive polygons (N = 16,890) and compared with variable availability in the valley bottoms. Based on mean values, Russian olive seems to prefer sandy soils over clay soils and grows closer to water, canal/ditches, forest and agriculture patches and to roads than could be expected based on availability (Table 4). Slope, valley width, salinity, pH, precipitations and % silt show less difference.

In addition, we graphed the distribution of the variables after grouping continuous variables into interval classes; results are presented over the following pages (Figure 9). Color scheme is the same for all graphs, with light green representing variable distribution within the valley bottoms and red representing variable distribution within Russian olive polygons. X axis is variable-specific and indicated below each graph; Y axis is percent.

Table 4. Value comparisons between Russian olive polygon centroids and variable availability within the study area, for 13 continuous variables.

Variable	Mean		Std Dev		Min		Max	
	VB	RO	VB	RO	VB	RO	VB	RO
Percent slope	1.878	1.7	3.89	3.03	0	0	1010.96	72.43
Valley width	3744.47	3506.53	1936.57	1782.99	101	178	9358	9358
Electric conductivity	2.52	2.63	3.65	3.94	0	0	31.9	31.9
pH	8.04	8	0.29	0.28	4.8	6.7	9.2	9.2
% clay	28.73	21.73	13.05	12.2	2.5	2.5	72.5	65.7
% sand	39.56	55.28	22.9	24.29	3.2	3.2	96.8	96.8
% silt	32.7	27.78	14.66	14.76	0.7	0.7	72.7	71.8
REAP	31.89	31.94	3.36	2.36	18	22	53	43
Distance to agriculture	431.26	321.51	1339.65	700.83	0	0	10000	10000
Distance to roads	773.09	624.81	1184.13	654.67	0	0	10000	10000
Distance to canal/ditch	1949.76	1226.12	2938.6	2069.93	0	0	10000	10000
Distance to forest	303.62	109.95	598.06	260.82	0	0	10000	10000
Distance to water	402.62	192.66	393.89	243.69	0	0	3110.9	2970.15

Based on these graphs, the topographical variables we used do not appear to influence the distribution of Russian olive (A, B, C). It seems to prefer areas of occasional flooding frequency (D), very sandy soils (%soil > 75%; F), and its distribution seems influenced by proximity to forested patches (distance < 50m; K) and water (<100m; N).

Maxent model

We entered the 16 variables and 4,469 training points into a Maxent model, leaving all user-defined parameters set to their default values with the exception of Maximum Number of Background Points, which was set to 50,000 (test runs with the default value of 10,000 gave lower accuracies).

The software generates a variety of outputs. Analysis of variable contribution shows that *distance to irrigated agriculture* has the greatest contribution to the model, followed by *distance to forest*, *distance to water*, and *flooding* (Table 5). In the Jackknife test of variable importance, *distance to agriculture* comes out again as being the environmental variable with the highest gain when used by itself, followed by *distance to forest*, *distance to water*, *% sand*, *% clay*, *% silt*, *texture,* and *flooding* (Figure 10). Both tests should be interpreted with caution when the predictor variables are correlated.

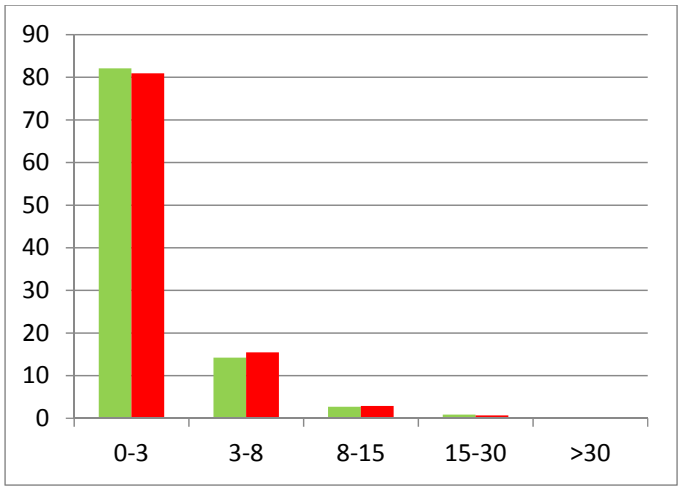

Figure 9A. Percent Slope

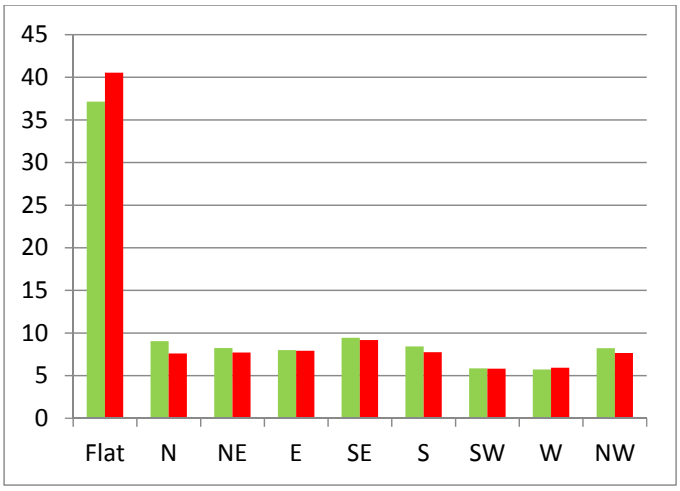

B. Aspect

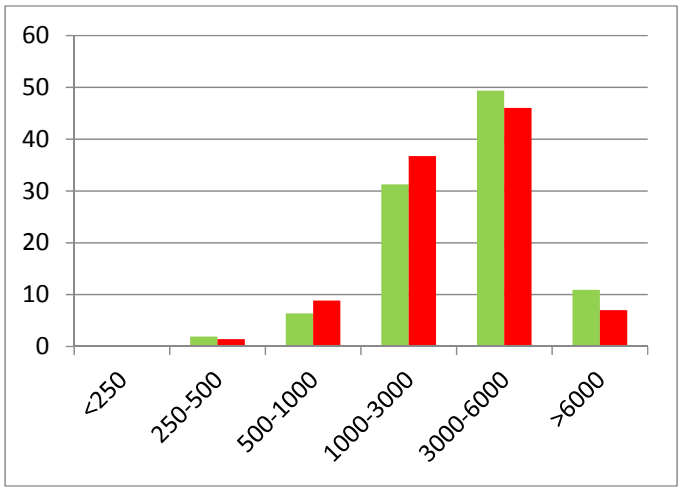

C. Valley Width (m)

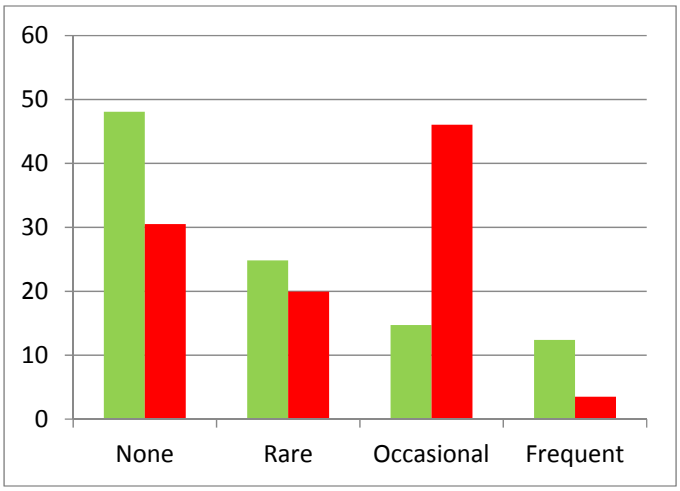

D. Flooding Frequency

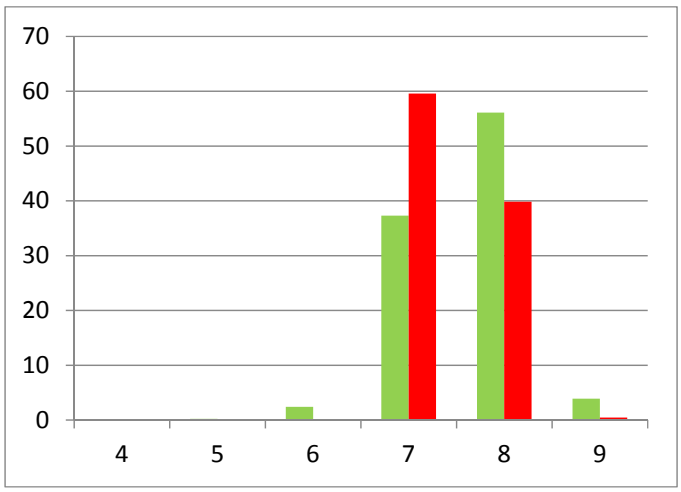

E. pH

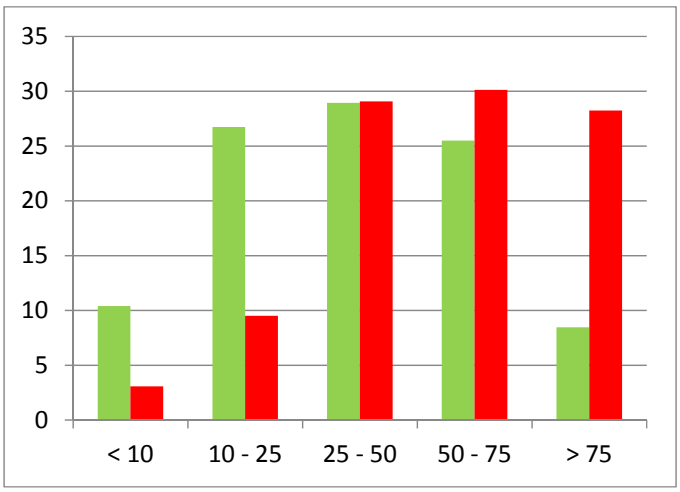

F. Percent Sand

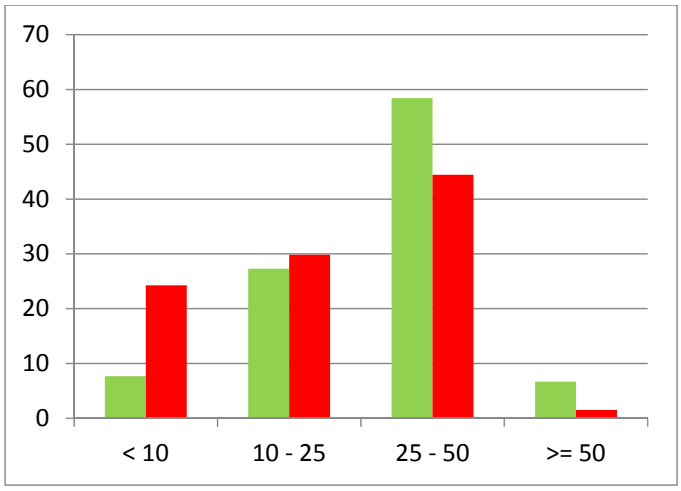

Figure 9G. Percent Clay

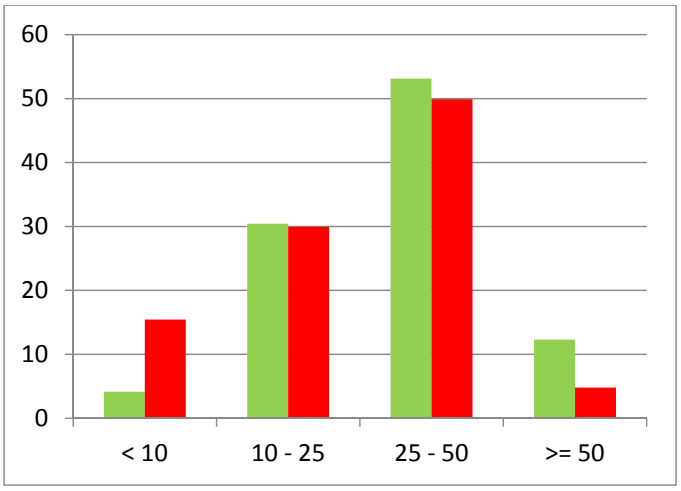

H. Percent Silt

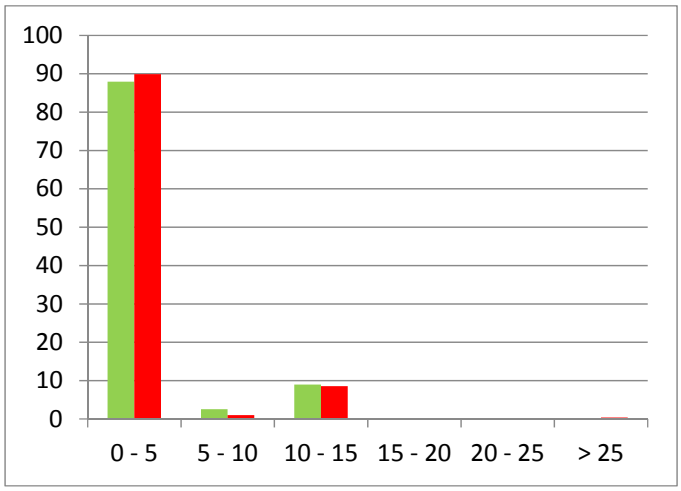

I. Electrical Conductivity

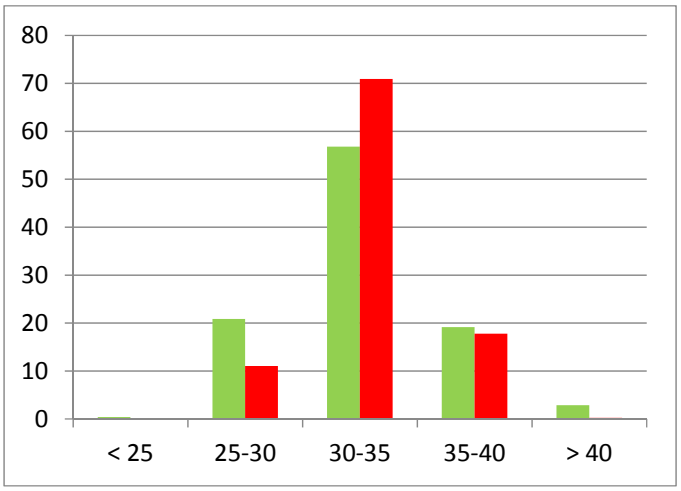

J. REAP

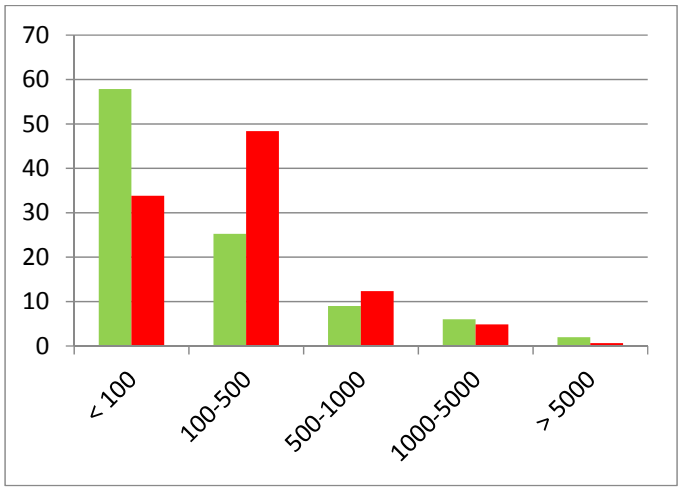

K. Distance to Irrigated Agriculture (m)

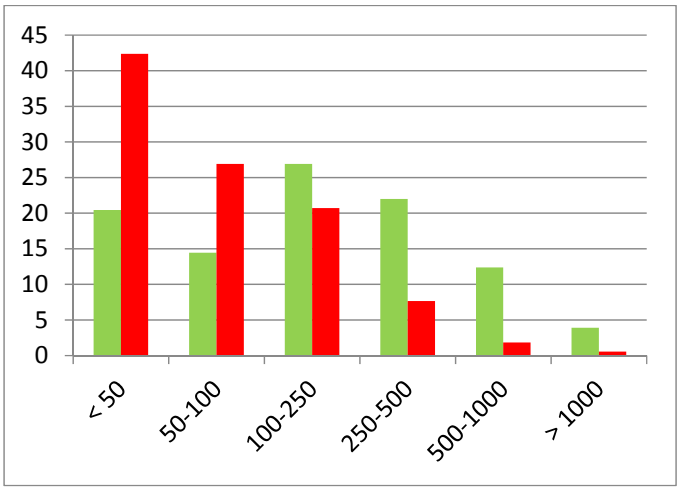

L. Distance to Forest (m)

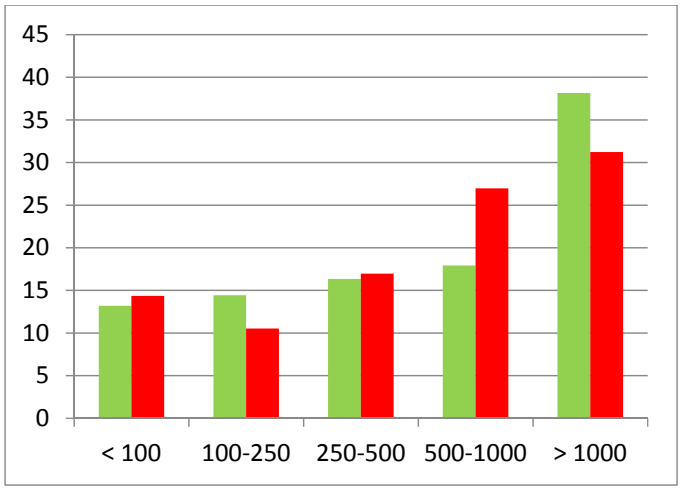

Figure 9M. Distance to Canal/Ditch (m)

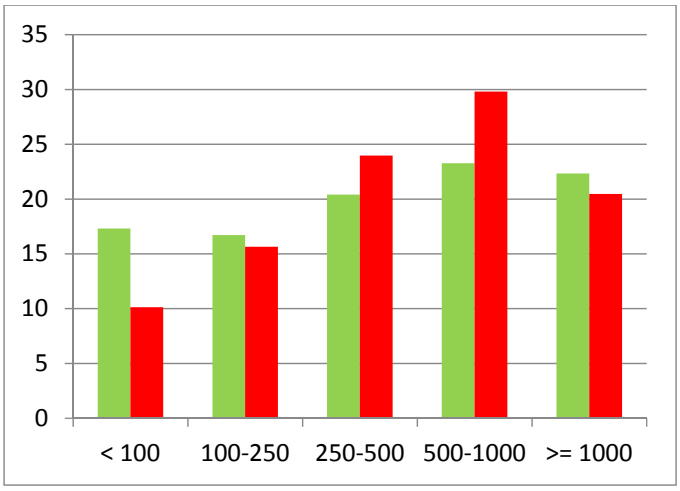

N. Distance to Roads (m)

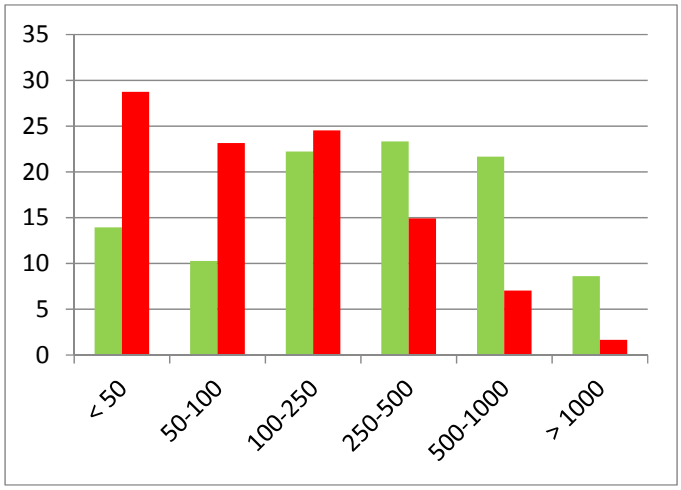

O. Distance to Water (m)

Figure 9. Histograms of 15 variables within Russian olive polygons (red) and study area (green).

Table 5. Relative contributions of the environmental variables to the Maxent model.

Variable	Percent Contribution
Distance to irrigated agriculture	41.5
Distance to forest	13.1
Distance to water	10.7
Flooding frequency	10.1
REAP	7.4
Distance to canal/ditch	4.5
Valley width	2.7
Percent clay	2.5
Distance to roads	2.4
Percent silt	1.5
Texture	1.5
Electrical conductivity	1
pH	0.6
Aspect	0.3
Slope	0.1
Percent sand	0.1

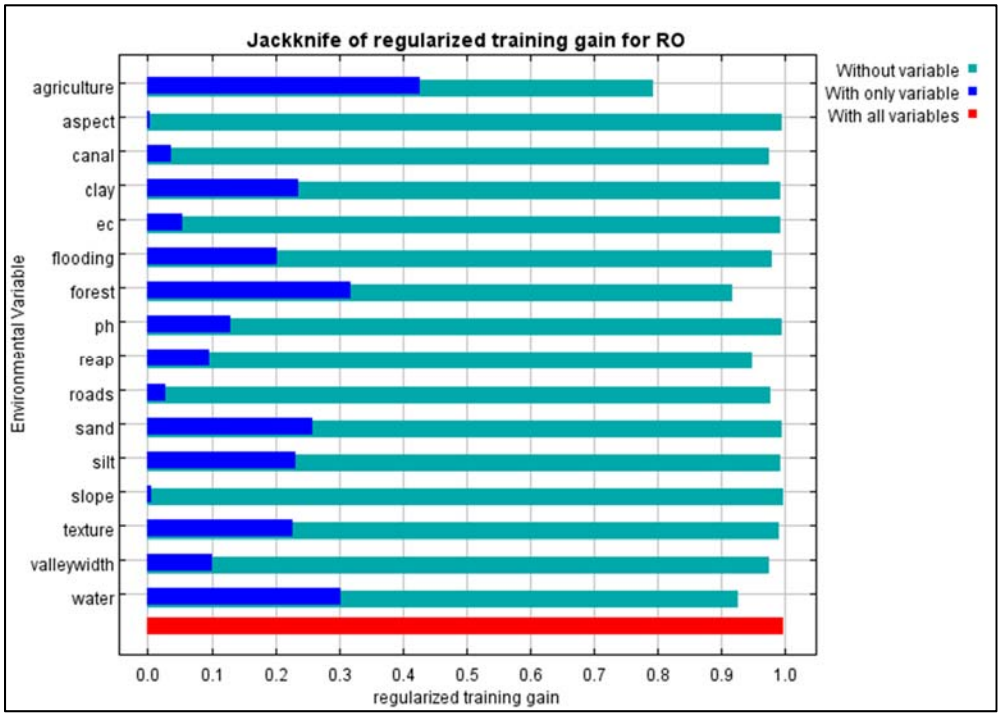

Figure 10. Jackknife of regularized training gain for Russian olive.

Classification accuracy is reflected in a Receiver Operating Characteristic (ROC) curve; the Area Under the Curve (AUC) ranges from 0.5 (random prediction) to 1 (perfect prediction). Our training data resulted in an AUC value of 0.878 and our test data in an AUC value of 0.877 (Figure 11).

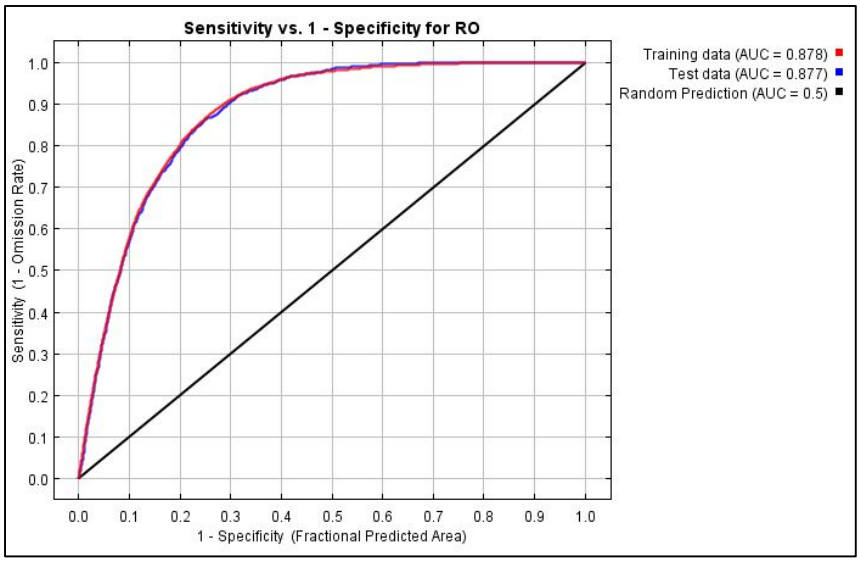

Figure 11. ROC curve showing the AUC for both training and test data.

When projected onto the environmental variables for the whole study area, the Maxent model is a continuous map of probability of presence (Figure 12), ranging from 0.00 to 0.9048, with a mean value of 0.1496 and a standard deviation of 0.1845.

Converting this continuous output into a binary, presence/absence output requires the selection of a logistic threshold (cut-off value) above which pixels will be classified as "suitable habitat" and below which they will be classified as "unsuitable habitat". Threshold selection procedures vary with the objectives of a particular analysis and affect prediction accuracy measures (Fielding and Bell 1997). Maxent outputs some common thresholds and corresponding omission rates (false negatives, i.e. true presences classified as absences) for both the training and test sets. A low threshold will result in higher sensitivity = a higher proportion of correctly predicted presence, but too low a threshold will result in the entire study area being classified as suitable habitat. Conversely, a higher threshold will result in higher specificity = a higher proportion of correctly predicted absence, but too high a threshold will fail to correctly classify existing Russian olive patches. A sample of threshold values output by Maxent ranged from 0.078 to 0.362, resulting in habitat acreage ranging from 220,216 acres to 684,513 acres; corresponding sensitivity values increased from 80% to 97.94% (Table 6). When deciding which threshold to use if a binary map is wanted, one needs to balance sensitivity and specificity. Here, we opted for a threshold value that maximizes training sensitivity plus specificity, i.e. 0.28 (Table 6, Figure 13).

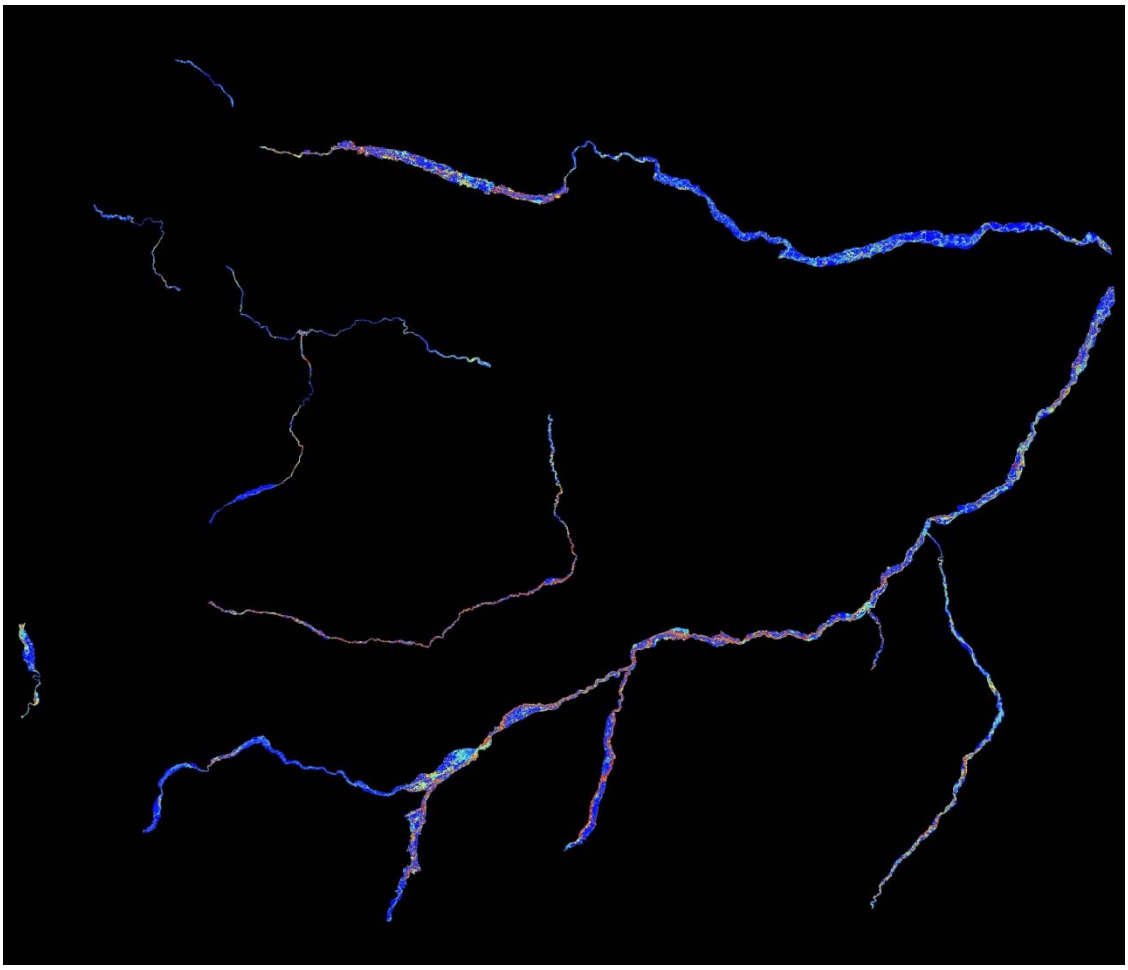

Figure 12. Russian olive Maxent model continuous output. Warmer colors show areas with better predicted conditions.

Table 6. Training and test data classification accuracy (% Russian olive polygon centroids correctly classified) and corresponding area of predicted suitable Russian olive habitat (acres) for different logistic threshold values.

Description	Threshold	Training	Test	Area
Balanced training omission, predicted area and threshold value	0.078	97.94	98.33	684,513
10 percentile training presence	0.250	90.04	88.84	349,830
Maximum training sensitivity plus specificity	0.280	87.89	86.50	310,235
Maximum test sensitivity plus specificity	0.297	86.17	85.70	289,801
Equal test sensitivity and specificity	0.358	80.62	79.55	224,162
Equal training sensitivity and specificity	0.362	80.00	79.34	220,216

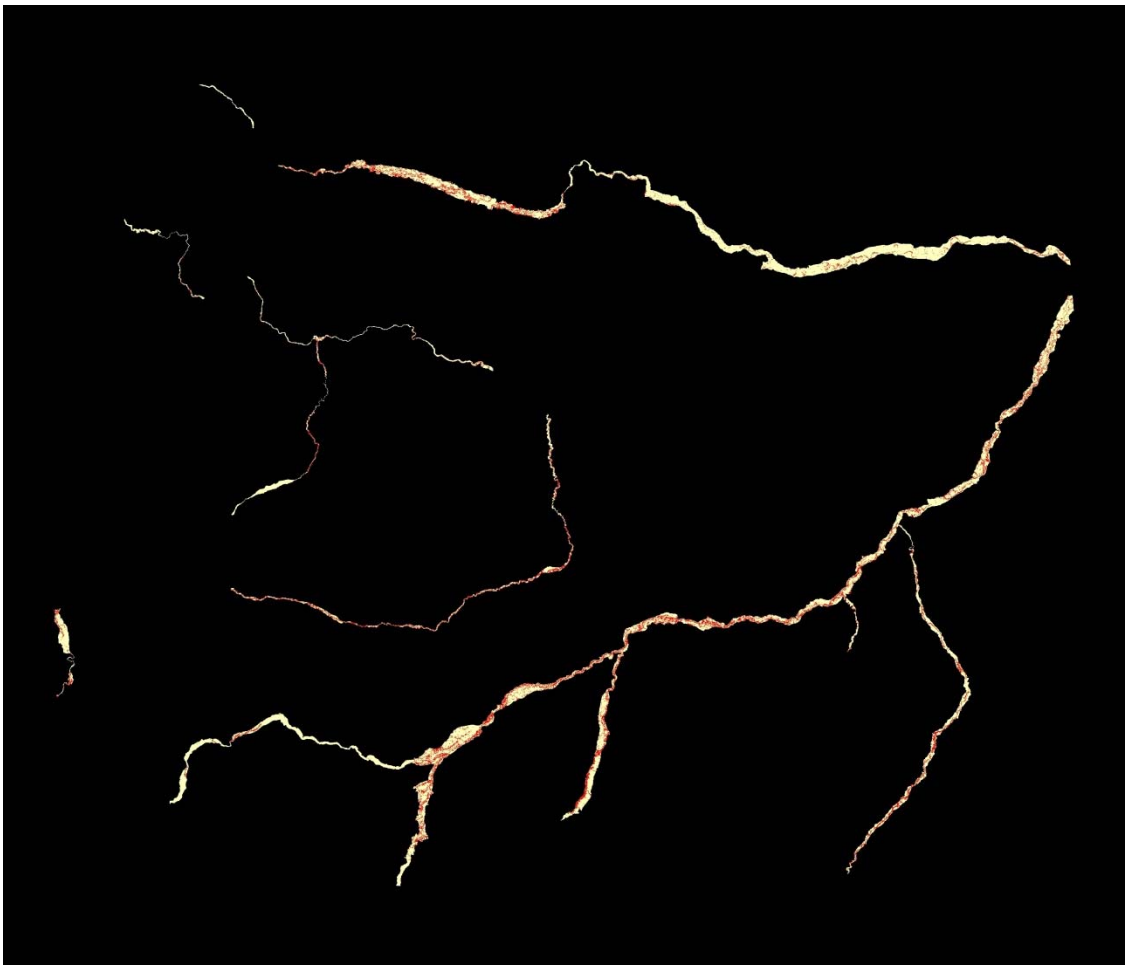

Figure 13. Russian olive Maxent model binary output. Red = high probability of Russian olive infestation.

Based on this binary map, acreage of current vs potential Russian olive infestation can be extracted on a river basis (Table 7). A total of 310,664 acres have a high probability of Russian olive infestation, representing a 17-fold increase over the current level of infestation. If a higher threshold is used, for example equal training sensitivity and specificity, potential Russian olive habitat would still be 12 times the size of current (220,216 acres vs 17,694 acres).

Another way to use the Maxent model output is to summarize its values for each polygon from the segmentation currently classified as Forested, Upland Emergent, Riparian Emergent, Shrub Scrub, or Sand Bar. For example, there are 4,075 (out of 723,913) polygons with a mean probability greater or equal to 75%, and 102,218 with a mean probability greater or equal to 50%.

Table 7. Current vs. modeled acreage of Russian olive in eastern Montana valley bottoms.

River	Current	Potential
Bighorn	2,607	22,802
Clark Fork of the Yellowstone	1,568	18,274
Judith	33	4,495
Marias	209	1,527
Milk	2,038	42,262
Missouri East	164	21,119
Missouri South	150	5,573
Missouri West	24	3,454
Musselshell	1,790	28,808
Powder	1,463	25,984
Tongue	46	2,011
Yellowstone	7,602	134,355
Sum	17,694	310,664

III. EVOLUTION OF RUSSIAN OLIVE DISTRIBUTION ALONG EASTERN MONTANA RIVERS

Anecdotal evidence from land managers and watershed stakeholders indicates that Russian olive eradication efforts are occurring throughout Montana, often with the goal of reducing a source population that might be contributing to downstream invasion. Because no single entity is charged with tracking these efforts or their results, we wanted to determine whether NAIP imagery from two different years can be used to follow the evolution of Russian olive encroachment, or its natural or artificial removal, along eastern Montana rivers.

Methods

Selection of imagery dates and test areas

NAIP was flown in Montana for the first time in 2005, with repeats in 2009, 2011, 2013 and 2015/16. Because it takes about 10 years for Russian olive trees to reach maturity and begin fruiting (Lesica and Miles 2001), the 10-year span between 2005 and 2015/16 NAIP should be sufficient to identify areas with new Russian olive colonization, or at least show growth/expansion of existing patches. A visual observation of NAIP along the Marias, where flow regulation by the Tiber Dam could lead to Russian olive eventually replacing cottonwood (Lesica and Miles 2001), shows that this appears to be the case (Figures 14, 15). However, it is difficult to know if Russian olive was genuinely absent from an area in 2005, or if the lower image quality makes its identification difficult (Figure 16).

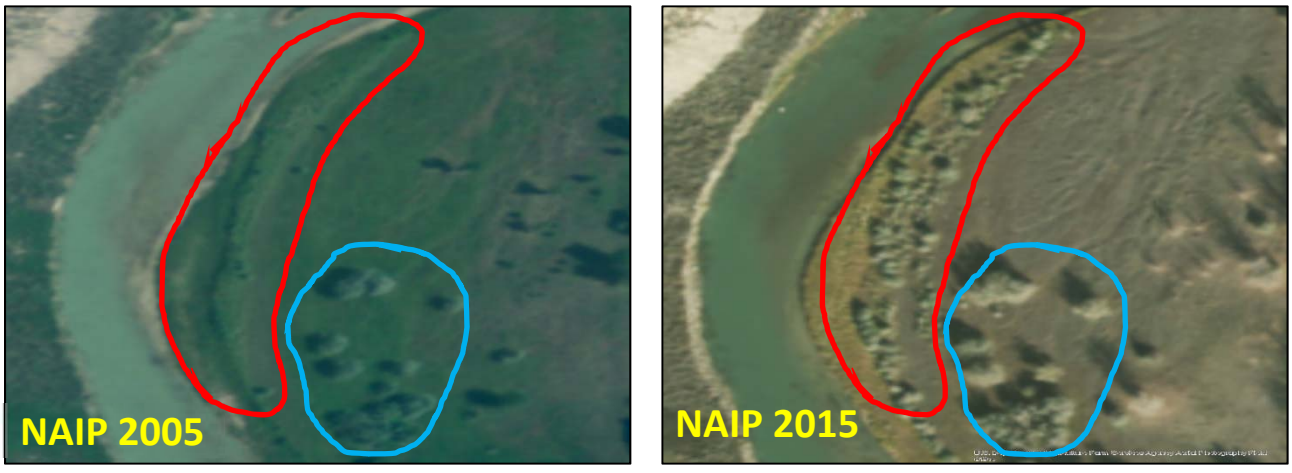

Figure 14. Evolution of Russian olive colonization along the Marias River, Montana, showing recruitment (red) and maintenance/growth of existing trees (blue).

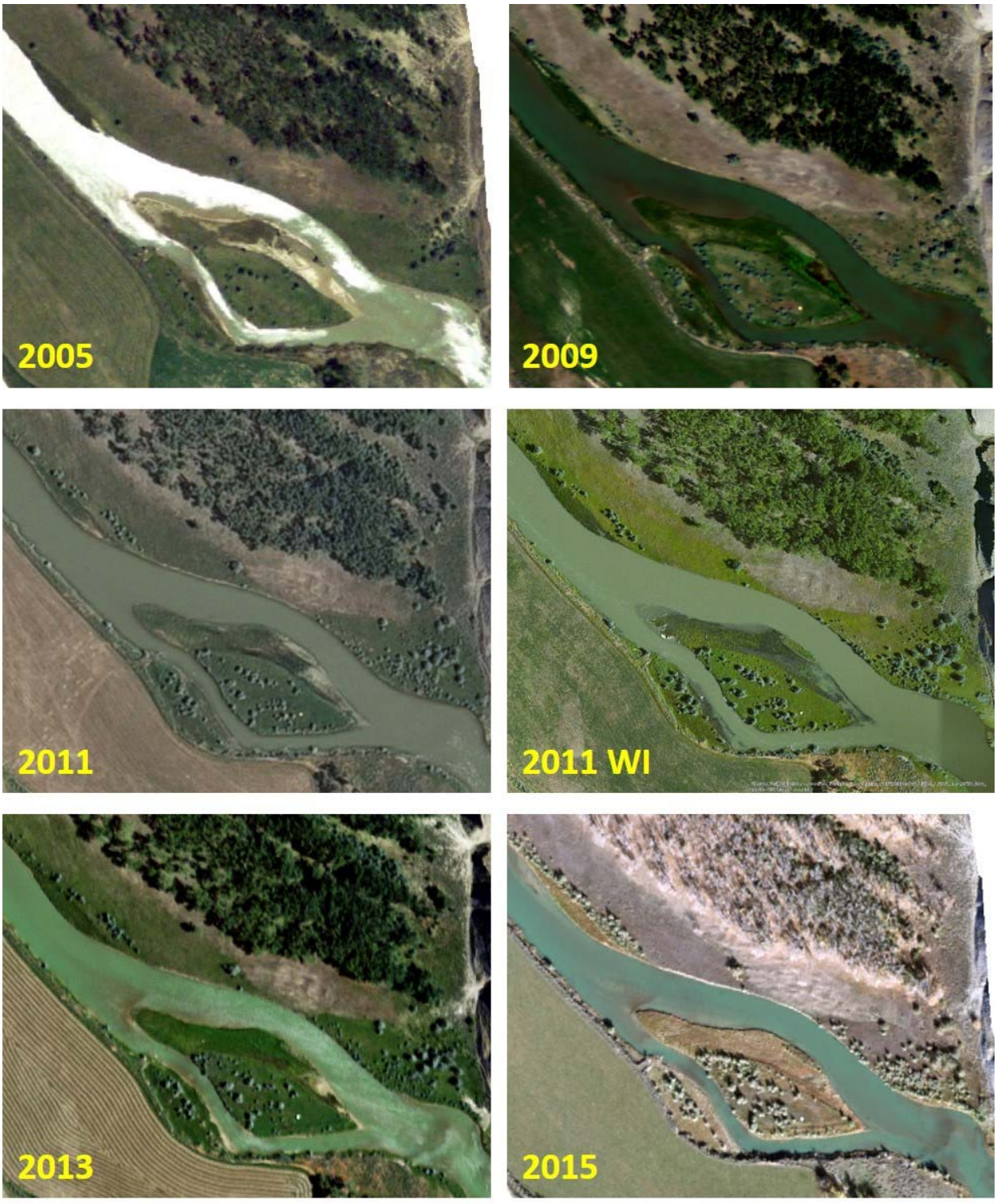

Figure 15. NAIP time series showing an example of Russian olive colonization/consolidation along the Marias River, Montana. 2011 WI is ESRI's 30cm resolution World Imagery (for comparison).

Figure 16. A comparison of 2005 and 2009 NAIP imagery highlights the difficulty of identifying young Russian olive trees in the 2005 imagery.

The pattern of Russian olive colonization along river banks also makes the species prone to removal by natural events, such as flooding along unregulated rivers. The 2011 floods in eastern Montana, which rerouted several river reaches (most notably the Mussellshell (Boyd et al. 2012; Figure 17)), would be expected to bring about such changes. Similarly, managers have been attempting to prevent the loss of riparian integrity and function associated with Russian olive infestation. For example, the Yellowstone River Conservation District Council stated three management objectives for Russian olive in the Yellowstone River system: 1) prevent new infestations; 2) eradicate all infestations within the river corridor; and 3) manage populations outside of the river corridor (YRCDC 2013). Although we could not find any direct reference to Russian olive removal along the Musselshell, we were interested to see if such management practices could be identified from NAIP imagery.

We opted for two different study areas and imagery sets. First, we undertook a comparison of 2005 and 2015 imagery along the Marias River, to assess whether areas of Russian olive recruitment could be identified despite 2005's lower quality imagery, and despite 2015's late date (85% September and 15% October). Second, we compared 2009 (pre-flooding) and 2015 (post-flooding) imagery along the Musselshell river, to assess whether areas of natural and/or human Russian olive removal could be identified. The Musselshell is also one of the few rivers that was partially flown in June (41.4%) and July (21%) in 2015.

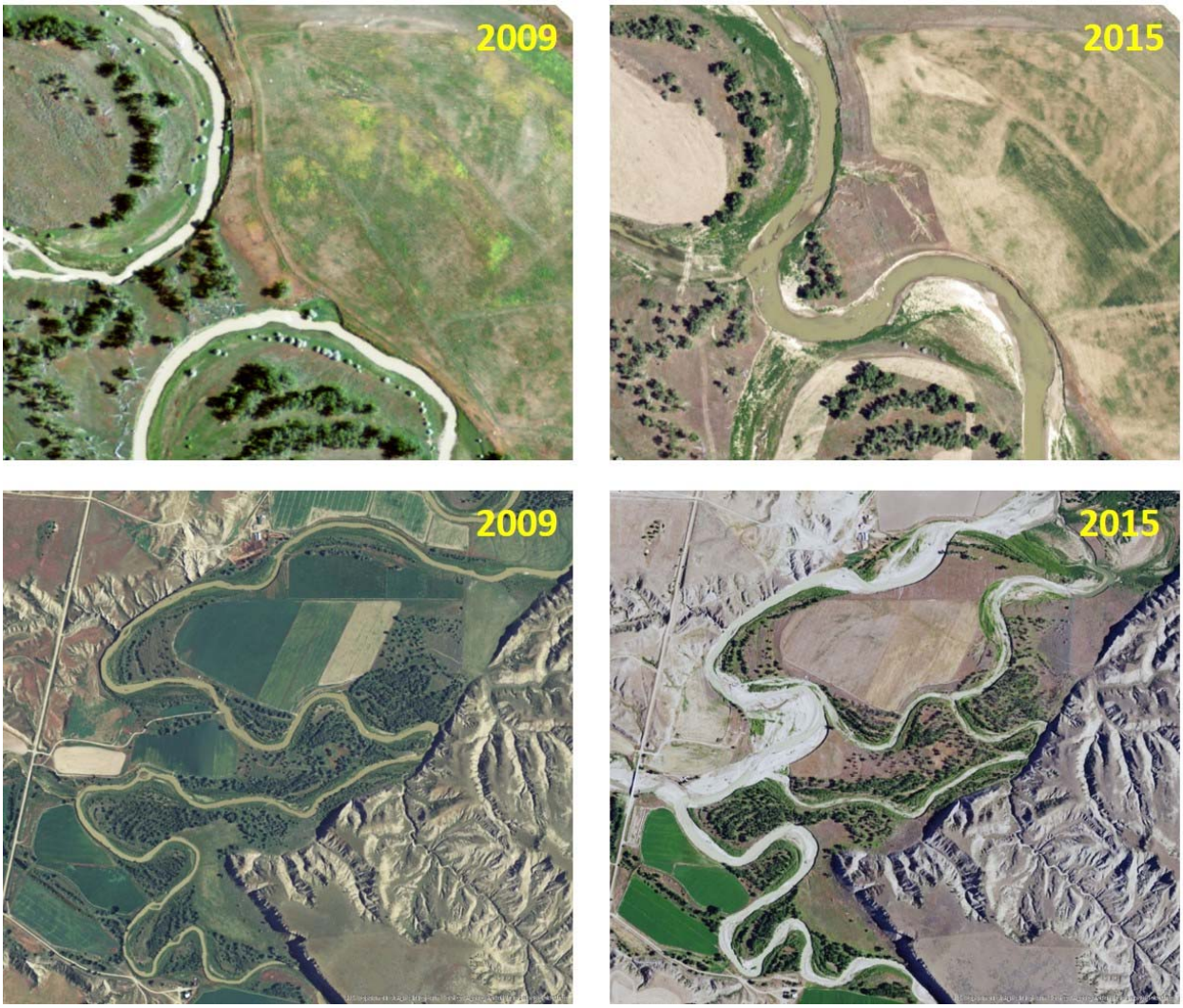

Figure 17. Examples of shifting river channel pre- and post-2011 flooding along the Musselshell River.

2005 – 2015 NAIP comparison along the Marias

After aggregating NAIP 2015 tiles in Erdas Imagine and extracting the 4-band imagery for the Marias valley bottom, we ran an eCognition multiresolution segmentation using the same parameters as in part I: Scale 100, Shape 0.3, Compactness 0.5. After segmenting, however, instead of running a RandomForest classification, we manually panned the valley bottom and selected those polygons containing Russian olive. These in turn were used to extract the four-band NAIP and a second segmentation was run, this time at a finer scale (25), to further separate Russian olive patches and even single Russian olive trees from other vegetation types (such as grass or bare ground) (Figure 18). Training points were digitized onscreen and an automated RandomForest classification (also using NDVI) was run in Weka. The same 35 attributes as in part I were used in the classification process, but a different set of training values were used: Russian olive, riparian grass, bare/dry grass, other shrubs/trees, and shadow, the latter necessary because a scale of 25 isolates tree shadows as individual polygons (Figure 18).

Figure 18. Example of two-step segmentation process along the Marias.

The fourth band (CIR) of NAIP 2005 was collected separately from the red-green-blue imagery, with some areas being flown in 2006, but this wasn't the case for the Marias so we used it in the segmentation/classification as though it had been collected simultaneously with the red-green-blue imagery. Classification followed the same methods as for 2015, but because of the sun angle, shadows were not as prevalent as in 2015. Thus, we used only 4 classes: Russian olive, bare/dry grass, riparian grass, and other shrubs/trees.

For both 2005 and 2015, we conducted visual post-modeling by panning over the valley bottom and manually reclassifying incorrect Russian olive polygons (errors of commission and omission). Although not necessarily repeatable over a very large area or for all cover types in a classification, this did not take long for the Russian olive along the Marias River.

2009 – 2015 NAIP comparison along the Musselshell

The methods described in 2.1 were repeated for the Musselshell, i.e., a two-step segmentation/classification process first using a scale of 100, then a finer scale of 25, based on 2009 and 2015 NAIP imagery. In addition to identifying all Russian olive polygons manually, we conducted a full classification at the 100 scale to capture the shifting river channel and quantify the extension of post-flooding sand bars. For both years, we used five classes (forested, riparian grass/shrub, upland grass/shrub, water, Russian olive); sand bars were also modeled in 2015 but were manually classified in 2009. Agriculture was added post-model by substituting polygons from the Montana Department of Revenue's most recent FLU dataset (DoR 2015).

Results

2005 – 2015 NAIP comparison along the Marias

Based on the internal validation provided by Weka, classification accuracy for Russian olive was high, above 90% for both years (Table 8). Manual post-modeling, conducted for Russian olive only, brought accuracy close to 100%. Because of the two-step modeling process, however, some isolated Russian olive trees, as well as some Russian olive interspersed among trees, were missed. But these constitute a small portion of Russian olive along the Marias.

Table 8. Internal accuracy results from a RandomForest classification of Russian olive along the Marias River, Montana.

	Russian olive user's accuracy	Russian olive producer's accuracy	Overall accuracy	Cohen's Kappa
2005	92.73%	91.07%	89.7%	0.8591
2015	93.11%	97.93%	90.79%	0.8704

In terms of acreage, the 2005 classification yielded 120 acres of Russian olive versus 150 acres in 2015, which is consistent with new colonization/expansion of existing patches. Combining the two datasets goes further by making it possible to identify areas mapped in 2005 only, in 2015 only, and both years (Table 9).

Table 9. Combination of Russian olive mapped in 2005 and 2015 along the Marias River.

Class	Acres
Mapped in 2005 only	54.5
Mapped in 2015 only	84.2
Mapped both years	65.7

Despite the overall greater acreage in 2015 compared to 2005 and the assumption that, along this regulated river, Russian olive coverage should have increased, there are areas where it has decreased, notably at the head of the river just below Tiber dam (Figure 19) Another example points out to active removal, possibly related to farming land management (Figure 20). In both cases, the model correctly picked out Russian olive in 2005. Conversely, patches of Russian olive mapped in 2015 but not in 2005 can easily be identified (Figure 21).

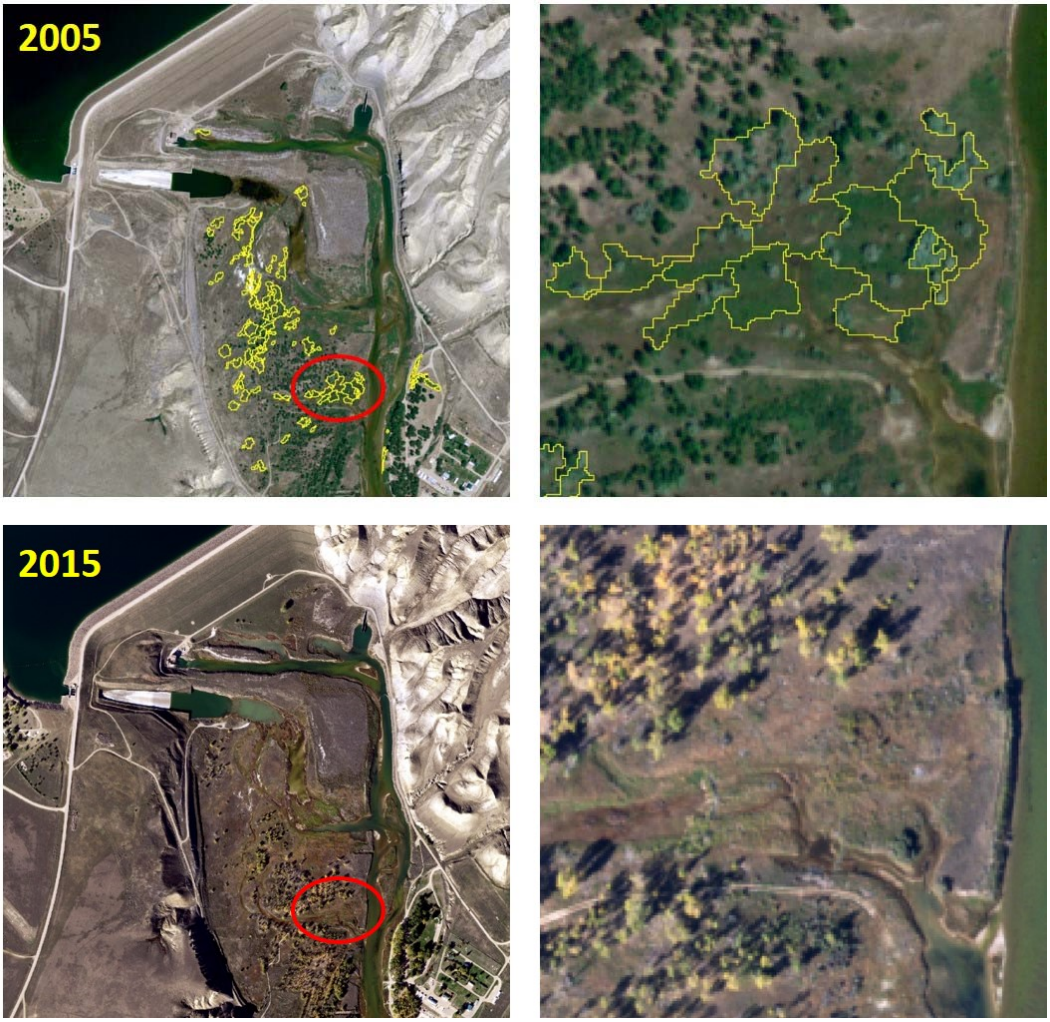

Figure 19. Russian olive patches below the Tiber dam on the Marias River in 2005 (above, with red circle area zoomed in) and their absence in 2015 (below).

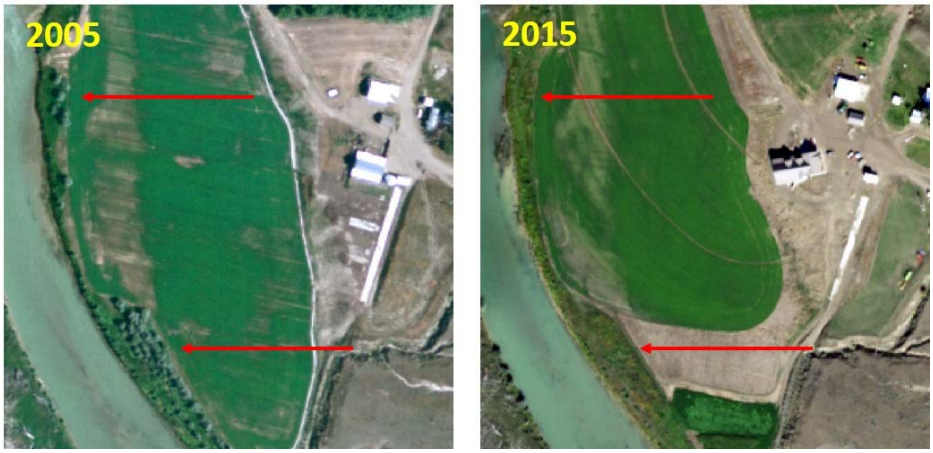

Figure 20. Russian olive patches present along the Marias River in 2005, but absent (active removal) in 2015.

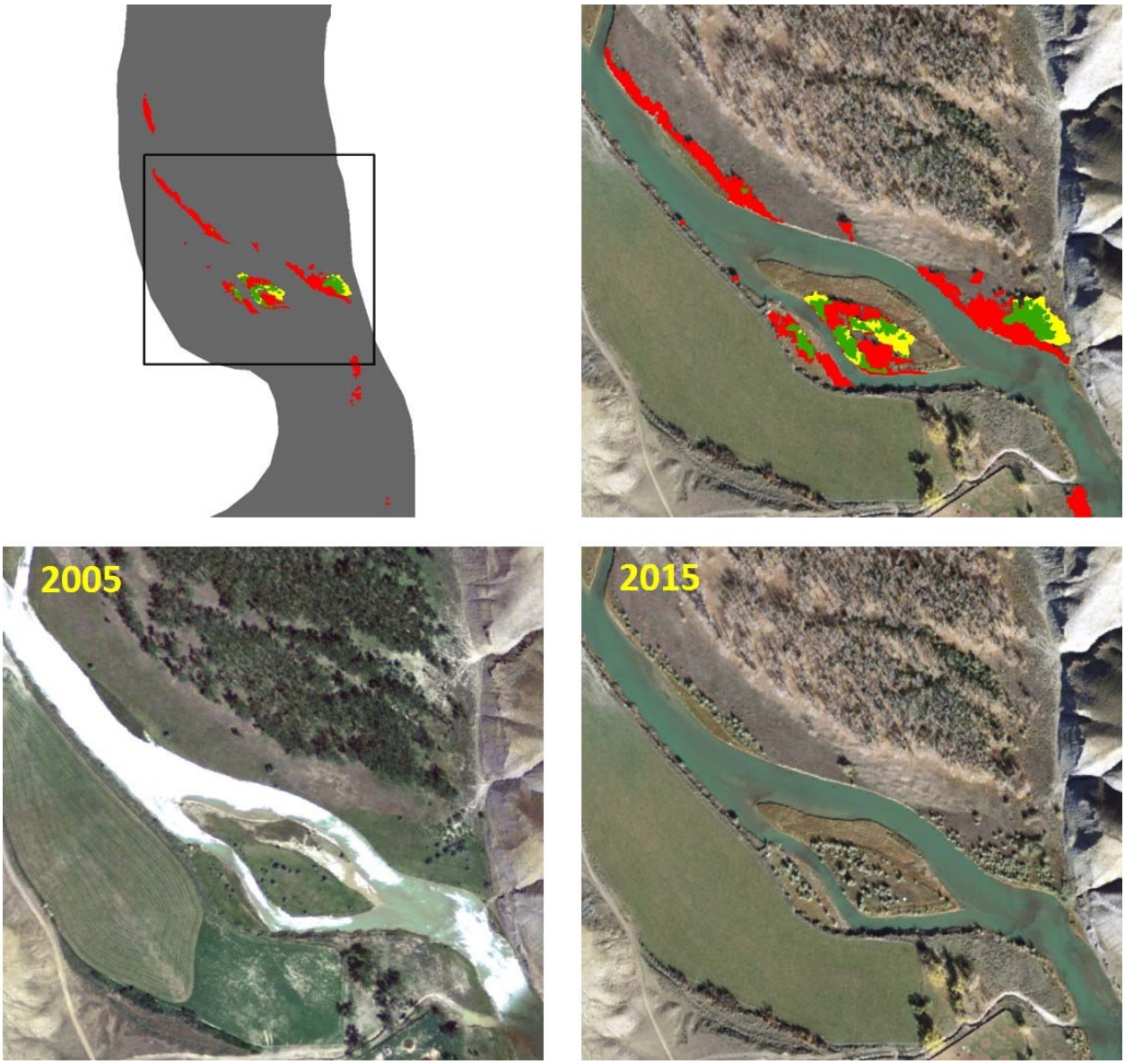

Figure 21. Comparison of Russian olive distribution along the Marias River between 2005 and 2015. Red polygons correspond to Russian olive mapped in 2015, but not in 2005; yellow polygons to patches mapped in 2005 only (probably a spurious result in this particular case, not the result of active removal); green polygons to patches mapped both years.

2009 – 2015 NAIP comparison along the Musselshell

Segmentation and classification at the 100 scale resulted in high classification accuracy based on internal validation (Table 10) and succeeded in mapping the shifting river course, sand bar creation/extension, and coarse-scale Russian olive patches (Figure 22). Acreage comparison between the two dates (Table 11) shows an impressive increase for sand bars (2612%!) and water (32%), and a substantial decrease (15%) for Russian olive, even taking into account potential misclassification errors and the coarseness of the mapping. Forest patches also show some decrease, but the decrease in riparian grassland and corresponding increase in upland grassland

can in part be explained by the fact that 2015 NAIP was flown in the fall, when grasses have dried up (i.e., it is spurious and a classification error).

Table 10. Internal accuracy results from a RandomForest classification along the Musselshell River, Montana.

	2009	2015
Forested (user's accuracy)	94.63	90.85
Riparian (user's accuracy)	90.43	94.21
Upland (user's accuracy)	92.36	90.38
Water (user's accuracy)	94.52	90.60
Russian olive (user's accuracy)	94.59	92.81
Sand bar (user's accuracy)	n/a	95.80
Overall accuracy	93.01	92.33
Cohen's Kappa	0.911	0.9079

Table 11. Acreage difference between 2009 and 2015 for 6 land cover types within the Musselshell valley bottom, based on NAIP imagery segmentation and classification.

Land cover type	2009	2015	Difference (acres)	Difference (%)
Agriculture	16,733	16,628	-105	- 0.63%
Forested	6,084	5,613	- 471	- 7.74%
Riparian	11,110	7,966	- 3,144	- 28.30%
Upland	8,638	10,772	+ 2,134	+ 24.70%
Sand bar	57	1,546	+ 1,489	+ 2,612%
Water	1,723	2,275	+ 552	+ 32.04%
Russian olive	3,027	2,571	+ 456	- 15.06

As was the case for the Marias River, the finer scale segmentation and classification done only for Russian olive patches helped "tighten" Russian olive distribution by separating the species from other vegetation types (Figure 23).

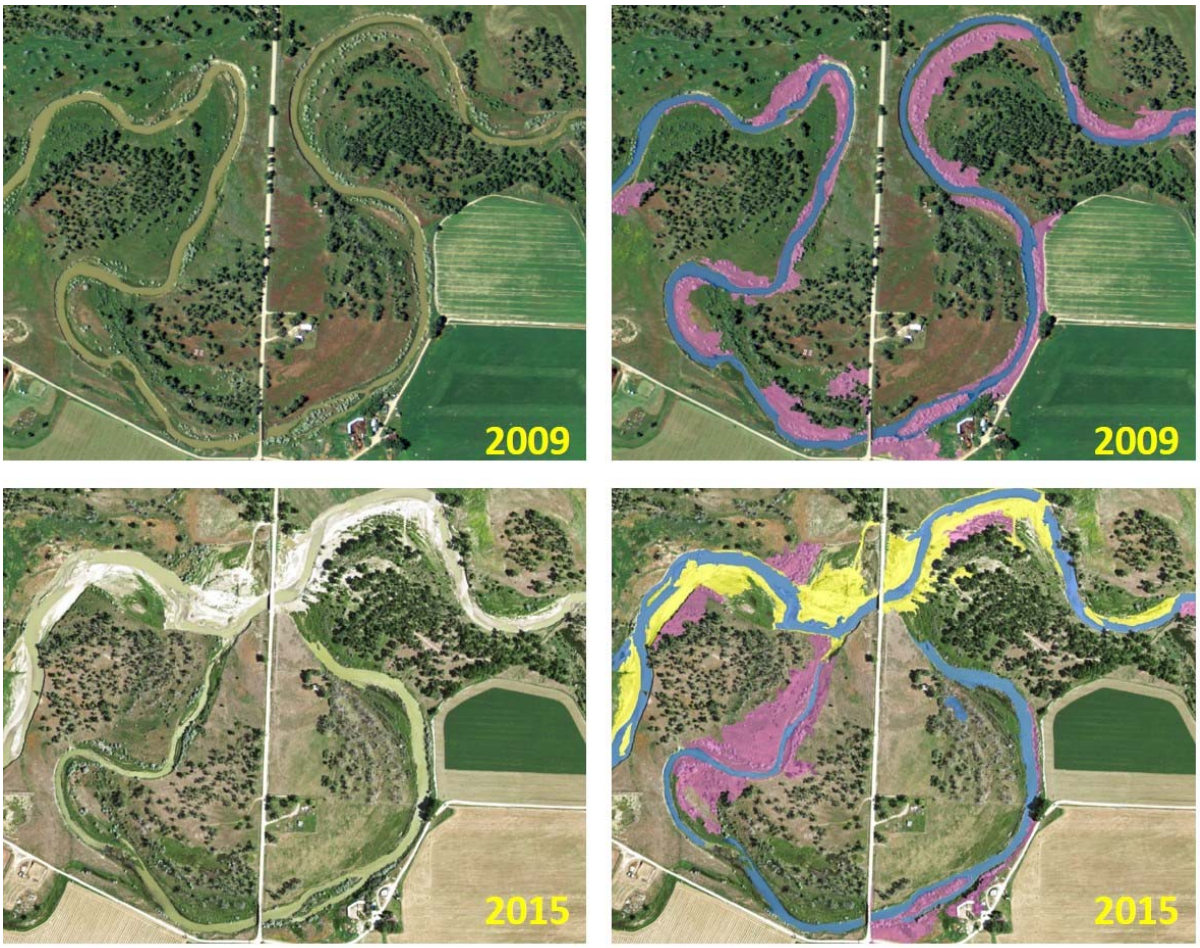

Figure 22. An example of classification of land cover as water (blue), sand bar (yellow) and Russian olive (pink) along the Musselshell River using 2009 and 2015 NAIP imagery.

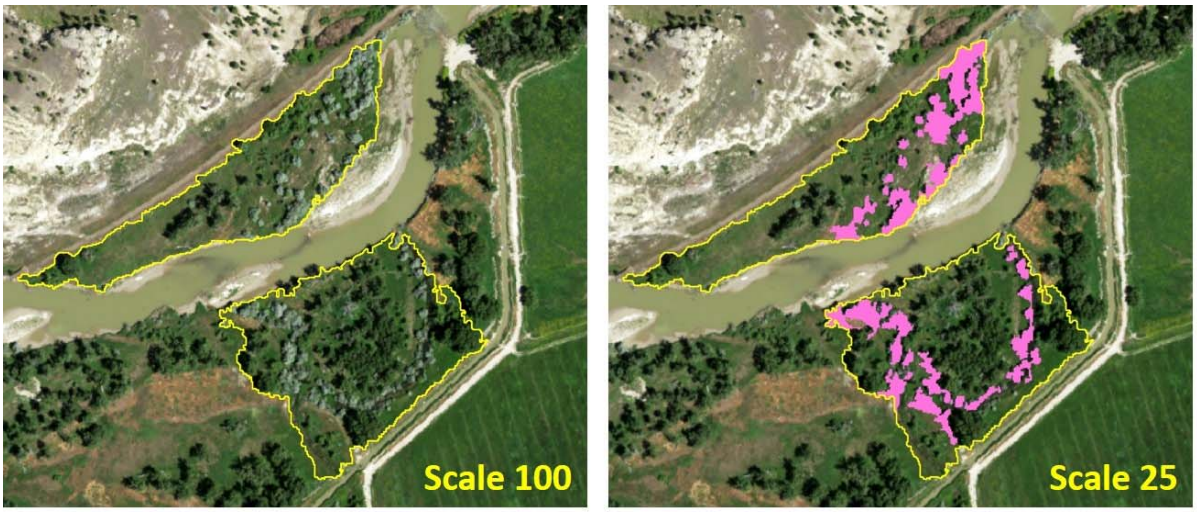

Figure 23. Example of two-step segmentation and classification process along the Musselshell River, targeting Russian olive. Yellow polygons: Russian olive at scale 100; pink polygons: Russian olive at scale 25.

Combining the two fine-scale maps of Russian olive results in 4 classes: mapped in 2009 only; mapped in 2015 only; mapped both years; mapped neither years (Table 12). Adding the common acreage of the two dates to each individual year results in 1,190 acres in 2009 vs 909 acres in 2015, a reduction of 23.61%. The first class (mapped in 2009 only) would correspond to those Russian olive patches or trees destroyed by the flood, or removed through active management; the second class (mapped in 2015 only), new Russian olive patches. This class, however, is likely to be spurious and the consequence of either omission error (the species was present in 2009 but missed by the mapping) or commission error (some other vegetation type was wrongly classified as Russian olive in 2015). The logical consequence, then, is to assume that all Russian olive mapped in 2015 was already there in 2009 and does not correspond to new colonization, resulting in the following acreage values: for 2009, 823 (mapped in 2009 only) + 541 (mapped in 2015) + 367 (mapped both years) = 1,731 acres; for 2015, 541 (mapped in 2015) + 367 (mapped in both) = 909 acres. This doubles the reduction of Russian olive between 2009 and 2015 (47.5%). The reality is probably somewhere between the two reduction values, to account for classification errors. Either way, there is still a significant amount of Russian olive reduction along the Musselshell River.

Table 12. Combination of Russian olive mapped in 2009 and 2015 along the Musselshell River.

Class	Acres
Mapped in 2009 only	823
Mapped in 2015 only	541
Mapped both years	367

After selecting those Russian olive patches mapped in 2009 but not in 2015, a visual inspection at a relatively fine scale (e.g. 1: 4,000) confirms the effect of the 2011 flood in removing the species along the river channel (Figure 24). It is also possible to detect recent, active management by the scars left on the landscape (Figure 25). When taking an overall view, one larger area emerged as having very little Russian olive in 2015 (Figure 26). Zooming in, it appears that this is most likely the result of active removal, as evidenced by the absence of major channel rerouting, the absence of Russian olive away from the river banks, and the presence of removal scars.

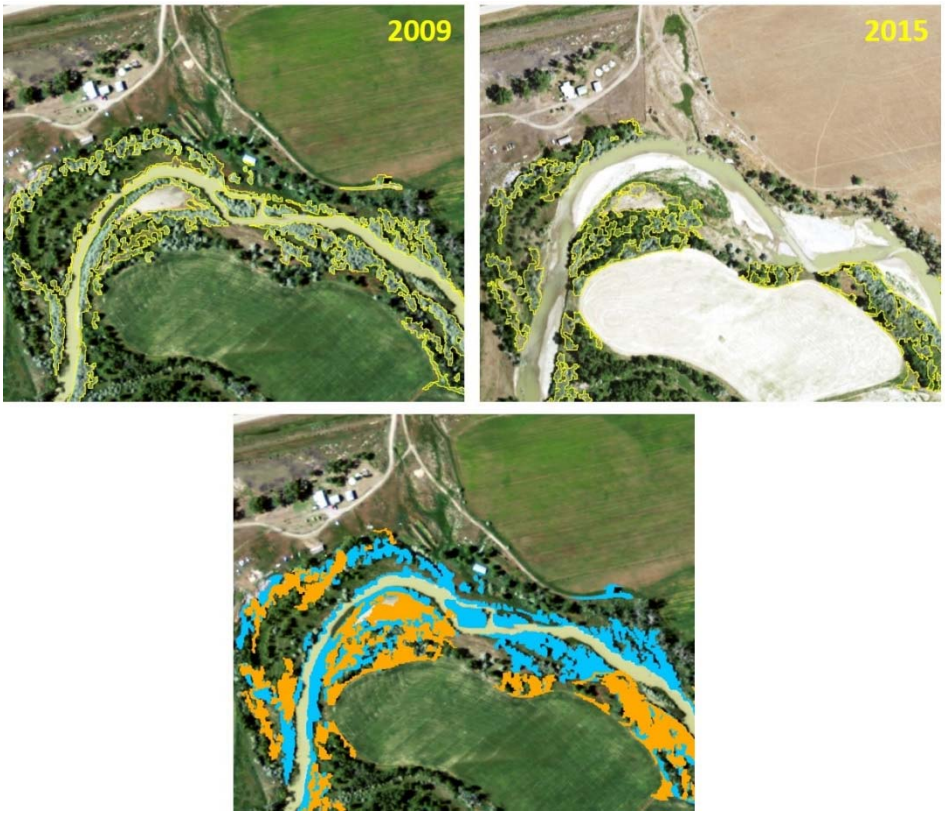

Figure 24. Effect of the 2011 flood on Russian olive along the banks of the Musselshell River. Orange polygons correspond to unaffected Russian olive (mapped both in 2009 and 2015), whereas blue polygons identify areas where Russian olive is no longer present.

Figure 25. Example of active Russian olive removal along the Musselshell River. The upper pictures show patches that the model classifies as Russian olive in 2009 but not in 2015; in the bottom picture, red arrows point to scars resulting from recent Russian olive removal.

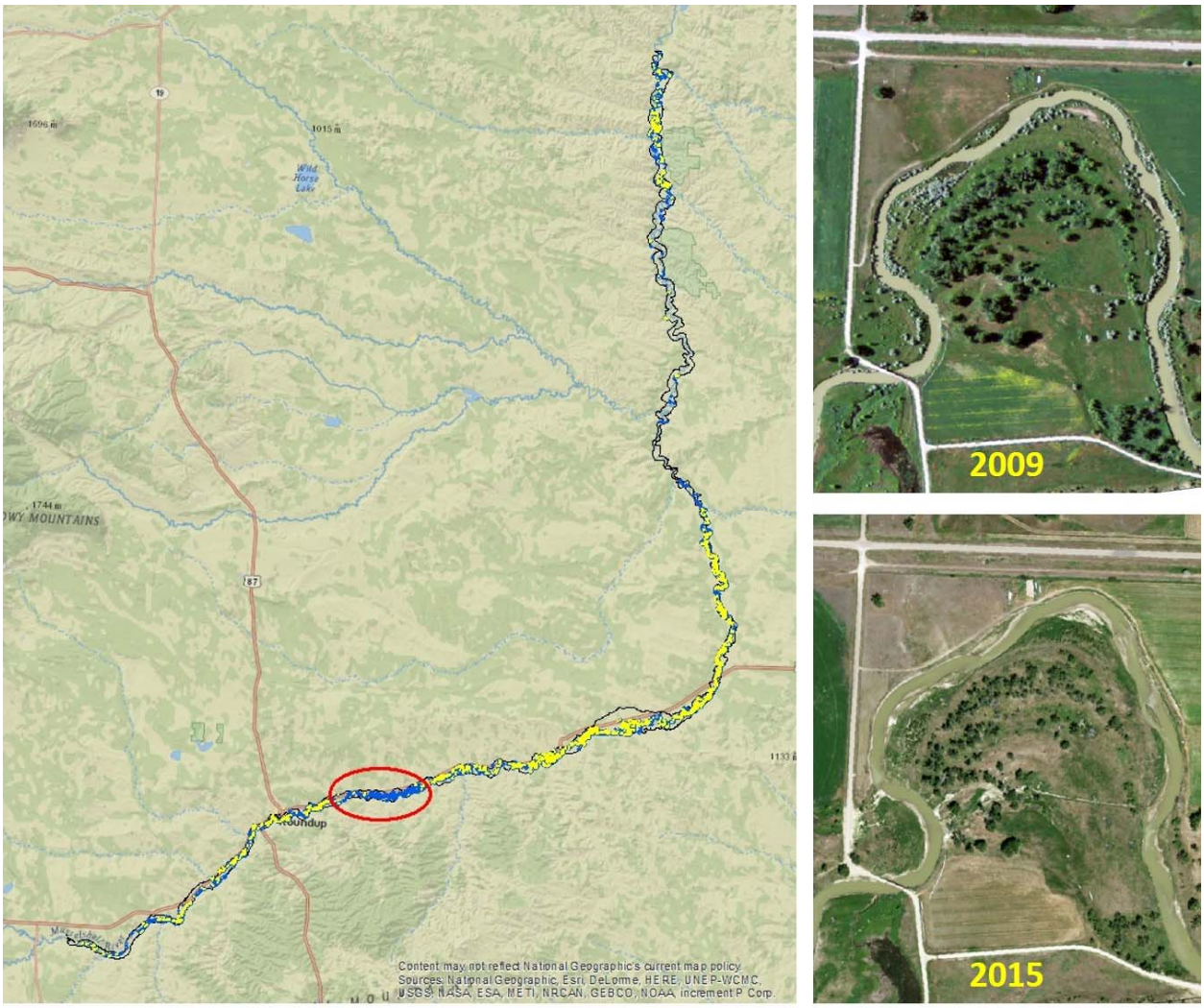

Figure 26. Overall comparison of Russian olive mapping along the Musselshell River between 2009 (blue) and 2015 (yellow), showing a section with Russian olive removal (red circle) and an example of zoomed-in imagery within it.

CONCLUSIONS

This study aimed at providing answers to the following questions:

I. Can NAIP be used to generate a current distribution map of Russian olive along eastern Montana rivers?
II. Can a predictive model of Russian olive infestation along eastern Montana rivers be developed and used to identify areas threatened by colonization?
III. Can NAIP be used to follow the evolution of the distribution of Russian olive along eastern Montana rivers? Evolution includes both increase (invasion of new sites, spatial expansion of established patches) and decrease (removal through natural flooding or through active management).

In Part I, we segmented NAIP 2013 imagery using eCognition and developed a RandomForest model to generate a land cover map of valley bottoms for ten eastern Montana rivers, Russian olive being one of the classes mapped. Classification accuracy for Russian olive was 75% or higher and made it possible to compare infestation among rivers. In Part II, we entered Russian olive data from Part I and 16 variables into Maxent to generate a predictive model of potential Russian olive infestation. Because it is a probabilistic model of future infestation, it is not possible to assess its accuracy, especially at the scale of entire valley bottoms. However, it can be used to direct attention to specific areas that could be more at risk of infestation than others. Finally, in Part III we focused on two rivers, the Marias (regulated) and the Musselshell (unregulated, subject to intense flooding episodes) to assess whether NAIP can be used to follow changes in Russian olive coverage. In both cases we found that NAIP imagery is accurate enough, even if it flown in late season, to pick up areas where Russian olive has been removed (either naturally through flooding, or through active management actions), as well as areas of expanded colonization. To reach a sufficient degree of accuracy at the patch level, however, required onscreen manual editing of the classification output. Nevertheless, the segmentation approach was faster than straight onscreen digitizing would be, and because of the scale of imagery (1m pixels), a better solution than a pixel-based classification.

Nationally, NAIP imagery is contracted each year based upon available funding; originally acquired on a 5-year cycle, it was updated to a 3-year cycle in 2008. For Montana it was most recently flown in 2015/16, so the next cycle will probably occur around 2018/19. Until then, fine-scale mapping like the one conducted in Part III could be repeated for other Montana rivers.

LITERATURE CITED

Booth, W.E., and J.C. Wright. 1959. Flora of Montana, part 2, dicotyledons. The Research Foundation at Montana State College, Bozeman.

Boyd et al. 2012. Musselshell River Flood Rehabilitation River Assessment Triage Team (RATT) Summary Report. MT DNRC.

Buddhika, M., P. Oduor, M. Anar, and L.A. Kotchman. 2013. Understanding factors that correlate or contribute to exotic Russian-olive (*Elaeagnus angustifolia*) invasion at a wildland-urban interface ecosystem. Invasive Plant Science and Management 6(1)130-139.

Buechling, A., and C. Tobalske. 2011. Predictive habitat modeling of rare plant species in Pacific Northwest forests. West. J. Appl. For. 26(2):71-81.

Christiansen, E.M. 1963. Naturalization of Russian olive (*Elaeagnus angustifolia* L.) in Utah. American Midland Naturalist 70:133–137.

Collette, L. 2014. An ecological assessment of Russian olive in western Canada: predicted distribution across its invaded range and insect associations in southern BC. Master's Degree Thesis, UBC.

Definiens AG. 2009. Definiens eCognition Developer 8 User Guide. Definiens AG: Munchen, Germany.

Elias, T.S. 1980. The complete trees of North America. Field guide and natural history. Van Norstrand Reinhold Co., New York.

Fielding, A.H., and J.F. Bell. 1997. A review of methods for the assessment of prediction errors in conservation presence/absence models. Environ. Conserv. 24(1):38-49.

Franklin, J., and J. A. Miller. 2009. Mapping species distributions: spatial inference and prediction. Cambridge Univ. Press, New York, NY.

Gao, Y., and J.F. Mas. 2008. A comparison of the performance of pixel based and object oriented classifications over images with various spatial resolutions. OnLine Journal of Earth Sciences 2(1):27-35.

Great Plains Flora Association. 1986. Flora of the Great Plains. University Press of Kansas, Lawrence.

Hoffman J., S. Narumalani, D. Mishra, P. Merani, and R. Wilson. 2008. Predicting potential occurrence and spread of invasive plant species along the North Platte River, Nebraska. Invasive Plant Science and Management 1(4):359-367.

Jarnevich, C., and L. Reynolds. 2011. Challenges of predicting the potential distribution of a slow-spreading invader: a habitat suitability map for an invasive riparian tree. USGS Staff – Published Research. Paper 734.

Lesica, P., and S. Miles. 2001. Natural history and invasion of Russian olive along eastern Montana rivers. Western North American Naturalist 61(1):1-10.

Lesica, P., and S. Miles. 2003. Russian olive invasion into cottonwood forests along a regulated river in north-central Montana. Can. J. Bot. 77:1077-1083.

Montana Department of Revenue. 2015. Revenue Final Land Unit (FLU) Classification. Helena, MT. Online link ftp://ftp.geoinfo.msl.mt.gov/Data/Spatial/NonMSDI/Geodatabases/revenue_flu.zip

Olson, T.E., and F.L. Knopf. 1986. Naturalization of Russian-olive in the western United States. Western Journal of Applied Forestry 1:65–69.

Pearce, C.M., and D.G. Smith. 2001. Plains cottonwood's last stand: can it survive invasion of Russian olive onto the Milk River, Montana floodplain? Environ. Manage. 28(5):623-637.

Peterson, A., M. Papes, and D. Kluza. 2003. Predicting the potential invasive distribution of four alien plant species in North America. Weed Science 51:863-868.

Phillips, S.J., R.P Anderson, and R.E. Schapire. 2006. Maximum entropy modeling of species geographic distributions. Ecol. Model. 190:231-259.

Woodbury, P.B., and D.A. Weinstein. 2010. Review of methods for developing regional probabilistic risk assessments, part 2: modeling invasive plant, insect, and pathogen species. In: Pye, John M.; Rauscher, H. Michael; Sands, Yasmeen; Lee, Danny C.; Beatty, Jerome S., tech. eds. Advances in threat assessment and their application to forest and rangeland management. Gen. Tech. Rep. PNW-GTR-802. Portland, OR: U.S. Department of Agriculture, Forest Service, Pacific Northwest and Southern Research Stations: 521-538.

Xie, Y., Z. Sha, and M. Yu. 2008. Remote sensing imagery in vegetation mapping: a review. J. Plant Ecol. 1(1): 9-23.

Yellowstone River Conservation District Council (YRCDC). 2013. Long-term strategy for Russian olive and saltcedar management. Report prepared by Thomas L. Pick, Bozeman, MT, 44 p. http://ftp.geoinfo.msl.mt.gov/Documents/Projects/Yellowstone_River_Clearinghouse/Russian_Olive_SaltCedar_Strategy_2013.pdf